15. Van Camp G, Flamez A, Cosyns B, et al. Treatment of Parkinson's disease with pergolide and relation to restrictive valvular heart disease. Lancet 2004;363:1179–1183.
16. Van Camp G, Flamez A, Cosyns B, Goldstein J, Perdaens C, Schoors D. Heart valvular disease in patients with Parkinson's disease treated with high-dose pergolide. Neurology 2003;61:859–861.
17. Pritchett AM, Morrison JF, Edwards WD, Schaff HV, Connolly HM, Espinosa RE. Valvular heart disease in patients taking pergolide. Mayo Clin Proc 2002;77:1280–1286.
18. Flowers CM, Racoosin JA, Lu SL, Beitz JG. The US Food and Drug Administration's registry of patients with pergolide-associated valvular heart disease. Mayo Clin Proc 2003;78:730–731.
19. Weber M, Hamm C. Role of B-type natriuretic peptide (BNP) and NT-proBNP in clinical routine. Heart 2006; 92:843–849.
20. Detaint D, Messika-Zeitoun D, Chen HH, et al. Association of B-type natriuretic peptide activation to left ventricular end-systolic remodeling in organic and functional mitral regurgitation. Am J Cardiol 2006;97:1029–1034.
21. Eimer MJ, Ekery DL, Rigolin VH, Bonow RO, Carnethon MR, Cotts WG. Elevated B-type natriuretic peptide in asymptomatic men with chronic aortic regurgitation and preserved left ventricular systolic function. Am J Cardiol 2004;94:676–678.
22. Watanabe H, Atsuta N, Ito M, et al. Relationship between non-motor function and quality of life in Parkinson's disease; longitudinal study. Rinsho Shinkeigaku 2007;47: 1015. Abstract.
23. Calne DB, Snow BJ, Lee C. Criteria for diagnosing Parkinson's disease. Ann Neurol 1992;32:S125–S127.
24. Junghanns S, Glöckler T, Reichmann H. Switching and combining of dopamine agonists. J Neurol 2004;251 suppl 6:VI/19–23.
25. Millan MJ, Maiofiss L, Cussac D, et al. Differential actions of antiparkinson agents at multiple classes of monoaminergic receptor: I: a multivariate analysis of the binding profiles of 14 drugs at 21 native and cloned human receptor subtypes. J Pharmacol Exp Ther 2002;303:791–804.
26. Jahnichen S, Horowski R, Pertz HH. Agonism at 5-HT2b receptor is not a class effect of the ergolines. Eur J Pharmacol 2005;513:225–229.
27. Zoghbi WA, Enriquez-Sarano M, Foster E, et al. Recommendations for evaluation of the severity of native valvular regurgitation with two-dimensional and Doppler echocardiography. J Am Soc Echocardiogr 2003;16:777–802.
28. McKee PA, Castelli WP, McNamara PM, et al. The natural history of congestive heart failure: the Framingham study. N Engl J Med 1971;285:1441–1446.
29. Ho KK, Anderson KM, Kannel WB, et al. Survival after the onset of congestive heart failure in Framingham Heart Study subjects. Circulation 1993;88:107–115.
30. Droogmans S, Franken PR, Garbar C, et al. In vivo model of drug-induced valvular heart disease in rats: pergolide-induced valvular heart disease demonstrated with echocardiography and correlation with pathology. Eur Heart J 2007;28:2156–2162.
31. Niinuma H, Nakamura M, Hiramori K. Plasma B-type natriuretic peptide measurement in a multiphasic health screening program. Cardiology 1998;90:89–94.
32. Nakamura M, Endo H, Nasu M, Arakawa N, Segawa T, Hiramori K. Value of plasma B type natriuretic peptide measurement for heart disease screening in a Japanese population. Heart 2002;87:131–135.
33. Redfield MM, Rodeheffer RJ, Jacobsen SJ, Mahoney DW, Bailey KR, Burnett JC Jr. Plasma brain natriuretic peptide concentration: impact of age and gender. J Am Coll Cardiol 2002;40:976–982.
34. Eguchi K, Kario K, Hoshide S, et al. Greater change of orthostatic blood pressure is related to silent cerebral infarct and cardiac overload in hypertensive subjects. Hypertens Res 2004;27:235–241.
35. Setola V, Hufeisen SJ, Grande-Allen KJ, et al. 3,4-Methylenedioxymethamphetamine (MDMA, "Ecstasy") induces fenfluramine-like proliferative actions on human cardiac valvular interstitial cells in vitro. Mol Pharmacol 2003;63:1223–1229.
36. Newman-Tancredi A, Cussac D, Quen-tric Y, et al. Differential actions of antiparkinson agents at multiple classes of monoaminergic receptor. III. Agonist and antagonist properties at serotonin, 5-HT(1) and 5-HT(2), receptor subtypes. J Pharmacol Exp Ther 2002;303:815–822.
37. Reichmann H, Bilsing A, Ehret R, et al. Ergoline and non-ergoline derivatives in the treatment of Parkinson's disease. J Neurol 2006;253 suppl 4:iv36–iv38.
38. Miller WL, Hartman KA, Burritt MF, et al. Serial biomarker measurements in ambulatory patients with chronic heart failure: the importance of change over time. Circulation 2007;116:249–257.
39. Detaint D, Messika-Zeitoun D, Avierinos JF, et al. B-type natriuretic peptide in organic mitral regurgitation: determinants and impact on outcome. Circulation 2005;111: 2391–2397.

Human Molecular Genetics, 2009, Vol. 18, No. 5 **898–910**
doi:10.1093/hmg/ddn419
Advance Access published on December 9, 2008

17-DMAG ameliorates polyglutamine-mediated motor neuron degeneration through well-preserved proteasome function in an SBMA model mouse

Keisuke Tokui[1,†], Hiroaki Adachi[1,*,†], Masahiro Waza[1], Masahisa Katsuno[1,2], Makoto Minamiyama[1], Hideki Doi[1], Keiji Tanaka[3], Jun Hamazaki[4], Shigeo Murata[4], Fumiaki Tanaka[1] and Gen Sobue[1,*]

[1]Department of Neurology, Nagoya University Graduate School of Medicine, 65 Tsurumai-cho, Showa-ku, Nagoya 466-8550, Japan, [2]Institute for Advanced Research, Nagoya University, 65 Tsurumai-cho, Showa-ku, Nagoya 466-8550, Japan, [3]Laboratory of Frontier Science, Core Technology and Research Center, Tokyo Metropolitan Institute of Medical Science, Bunkyo-ku, Tokyo 113-8613, Japan and [4]Laboratory of Protein Metabolism, Graduate School of Pharmaceutical Sciences, University of Tokyo, 7-3-1 Hongo, Bunkyo-ku, Tokyo 113-0033, Japan

Received October 1, 2008; Revised November 13, 2008; Accepted December 5, 2008

The ubiquitin–proteasome system (UPS) is the principal protein degradation system that tags and targets short-lived proteins, as well as damaged or misfolded proteins, for destruction. In spinal and bulbar muscular atrophy (SBMA), the androgen receptor (AR), an Hsp90 client protein, is such a misfolded protein that tends to aggregate in neurons. Hsp90 inhibitors promote the degradation of Hsp90 client proteins via the UPS. In a transgenic mouse model of SBMA, we examined whether a functioning UPS is preserved, if it was capable of degrading polyglutamine-expanded mutant AR, and what might be the therapeutic effects of 17-(dimethylaminoethylamino)-17-demethoxygeldanamycin (17-DMAG), an oral Hsp90 inhibitor. Ubiquitin-proteasomal function was well preserved in SBMA mice and was even increased during advanced stages when the mice developed severe phenotypes. Administration of 17-DMAG markedly ameliorated motor impairments in SBMA mice without detectable toxicity and reduced amounts of monomeric and nuclear-accumulated mutant AR. Mutant AR was preferentially degraded in the presence of 17-DMAG in both SBMA cell and mouse models when compared with wild-type AR. 17-DMAG also significantly induced Hsp70 and Hsp40. Thus, 17-DMAG would exert a therapeutic effect on SBMA via preserved proteasome function.

INTRODUCTION

Polyglutamine (polyQ) diseases are inherited neurodegenerative disorders caused by the expansion of trinucleotide repeats in the causative genes (1). One of these is spinal and bulbar muscular atrophy (SBMA), characterized by premature muscular exhaustion, progressive muscular weakness, atrophy and fasciculation in bulbar and limb muscles (2). In SBMA, a CAG repeat with 14–32 CAGs expands to 40–62 CAGs in the first exon of the androgen receptor (AR) gene (3). Pathological findings of SBMA are lower motor neuronal loss (4) and diffuse nuclear accumulations and nuclear inclusions (NIs) of polyQ-expanded mutant AR in the residual motor neurons in the brainstem and spinal cord as well as in some other visceral organs (5).

Heat shock protein 90 (Hsp90), a cytosolic molecular chaperone, is involved in the maturation and activation of a number of proteins, known as client proteins. Hsp90 client proteins comprise numerous oncoproteins (6) and steroid receptors, including AR (7). Hsp90 inhibitors enhance the proteasomal degradation of

*To whom correspondence should be addressed. Tel: +81 52-744-2385; Fax: +81 52-744-2384; Email: hadachi@med.nagoya-u.ac.jp; sobueg@med.nagoya-u.ac.jp
†The authors wish it to be known that, in their opinion, the first two authors should be regarded as joint First Authors.

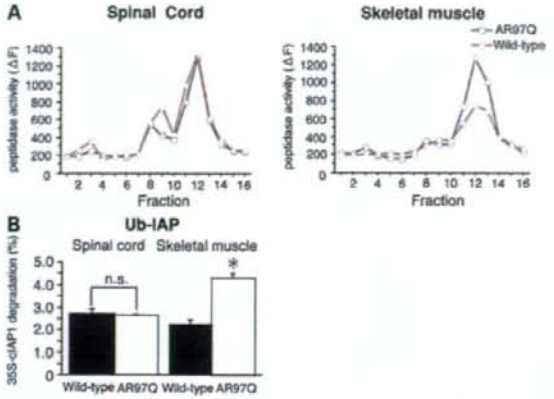

Figure 1. Protein-degrading activity of proteasomes. (**A**) Chymotryptic activity of 26S proteasomes in AR-97Q (SBMA) and AR-24Q (wild-type) mice. (**B**) Ubiquitin-dependent degradation of 35S-labeled cIAP1 in AR-24Q (wild-type) and AR-97Q mice. Data are mean ± SE from triplicate experiments. $^{*}P < 0.005$.

the Hsp90 client proteins, particularly of their mutant versions (8). Additionally, Hsp90 inhibitors also function as Hsp inducers (9). Therefore, numerous oncoproteins belonging to the Hsp90 client protein family are selectively degraded in the ubiquitin–proteasome system (UPS) by Hsp90 inhibitors. 17-(dimethylaminoethylamino)-17-demethoxy-geldanamycin (17-DMAG; NSC707545), a potent Hsp90 inhibitor, is now under clinical trials as a novel molecular-targeted agent for a wide range of malignancies (10). Recently, we explored the possibility of using 17-allylamino-17-demethoxygeldanamycin (17-AAG; NSC-330507), another Hsp90 inhibitor, as a therapeutic agent for SBMA and found that 17-AAG inhibits nuclear accumulation of the mutant AR protein, leading to marked amelioration of the motor phenotype of the transgenic mouse model of SBMA (AR-97Q mice) without detectable toxicity (11). 17-DMAG is a more potent derivative of 17-AAG (12,13), is more water soluble than 17-AAG and can be administered orally (14), thus possibly making it a more feasible long-term therapeutic agent for treating SBMA.

Hsp90 inhibitor-induced client protein degradation requires a well-preserved proteasome function; however, the question of whether the UPS is impaired in patients with polyQ diseases has been raised with respect to this UPS-dependent therapy (15). It is generally considered that the UPS is involved in polyQ diseases, as many components of the UPS and molecular chaperones are known to co-localize with polyQ-containing NIs (16,17). Nevertheless, previous studies using proteasome assays performed in cultured cell and mouse models of polyQ diseases have not shown consistent results; the UPS was impaired in some (18–24) and preserved in others (25–29). If the UPS is irreversibly damaged in patients and animal models of polyQ diseases, Hsp90 inhibitors cannot exert their pharmacological effects. Thus, it is important to assess whether the UPS is impaired, particularly in *in vivo* models of polyQ diseases with advanced phenotypic expressions. In this study, we employed multiple assessments to investigate whether the UPS function is preserved in transgenic AR-97Q SBMA mice and examined the effects of 17-DMAG on the phenotypic expression of SBMA in these mice.

RESULTS

Proteasomal proteolytic activity is preserved in AR-97Q mice with advanced phenotypes

To investigate proteasome functions, the chymotryptic activity of the proteasome was examined in AR-24Q (wild-type AR) and AR-97Q (mutant AR) mice at an advanced stage (16 weeks) (30). Most 16-week-old AR-97Q mice developed the severe phenotype. Chymotryptic activities of the 26S proteasomes in the AR-97Q mice were similar to wild-type in the spinal cord (Fig. 1A, left) and increased with respect to wild-type in skeletal muscle (Fig. 1A, right). We also examined ubiquitin-dependent proteolytic activity using 35S-labeled ubiquitinated cIAP1, a ubiquitin ligase that catalyzes its own ubiquitination for degradation. The levels of ubiquitin-dependent degradation in spinal cord of AR-97Q mice were not significantly different from wild-type (Fig. 1B, left); in skeletal muscle, however, degradation was higher in the AR-97Q mice than in the wild-type mice (Fig. 1B, right). These assays indicate that proteasomal function in AR-97Q mice with severe phenotypes was preserved in the spinal cord and was enhanced in skeletal muscle.

Proteasomal function in Ub^{G76V}-GFP/AR-97Q reporter mice is preserved

The Ub^{G76V}-GFP mouse was developed as an *in vivo* reporter of UPS function (31). They express an N-terminal ubiquitin mutant (Ub^{G76V}) in frame with enhanced green fluorescent protein (32). As the reporter is rapidly processed and degraded by the UPS, steady-state levels of Ub^{G76V}-GFP are very low under wild-type conditions, but accumulate when the UPS is impaired. We evaluated levels of Ub^{G76V}-GFP in spinal cord and skeletal muscle lysates of double transgenic, Ub^{G76V}-GFP/AR-97Q and Ub^{G76V}-GFP/AR-24Q mice (see Supplementary Material). Immunoblot analyses showed that Ub^{G76V}-GFP in the AR-97Q mice was increased in the spinal cord (30%) and skeletal muscle (85%) compared with AR-24Q mice (Fig. 2A). These results were well correlated

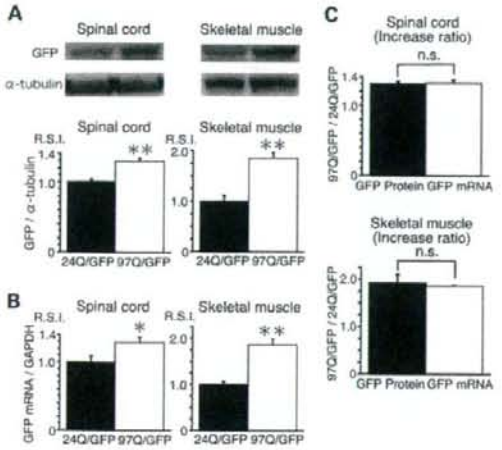

Figure 2. Ub^{G76V}-GFP reporter expression levels in the spinal cord and skeletal muscle of 16-week-old AR-24Q and AR-97Q mice. (**A**) Quantification of Ub^{G76V}-GFP protein levels by western blot relative to α-tubulin in the spinal cord and skeletal muscle of Ub^{G76V}-GFP/AR-24Q and Ub^{G76V}-GFP/AR-97Q mice. (**B**) Quantification of Ub^{G76V}-GFP mRNA levels relative to GAPDH by real-time RT–PCR analysis in the spinal cord and skeletal muscle of Ub^{G76V}-GFP/AR-24Q and Ub^{G76V}-GFP/AR-97Q mice. Values in (A) and (B) are expressed as mean ± SE, $n = 6$; $^{*}P < 0.05$; $^{**}P < 0.0005$. (**C**) The relative increases in Ub^{G76V}-GFP protein and mRNA levels in Ub^{G76V}-GFP/AR-24Q and Ub^{G76V}-GFP/AR-97Q mice. $n = 6$.

with those of anti-GFP immunohistochemical-stained tissue sections (compare with Supplementary Material, Fig. S1A and C).

To assess whether the increases in reporter levels reflect UPS function or reporter mRNA expression levels, we quantified mRNA levels of Ub^{G76V}-GFP by real-time RT–PCR and noted increases in Ub^{G76V}-GFP mRNA levels in Ub^{G76V}-GFP/AR-97Q mice compared with those in Ub^{G76V}-GFP/AR-24Q mice (Fig. 2B). The increases in protein levels were very similar to those in mRNA levels (Fig. 2C), strongly indicating that the increases in reporter proteins in the spinal cord and muscle were due to increased expressions of reporter protein mRNAs and that UPS function is well preserved in AR-97Q mice even in their advanced stage. Furthermore, *in situ* hybridization (Supplementary Material) also demonstrated an increase in Ub^{G76V}-GFP reporter mRNA levels in the spinal motor neurons and skeletal muscle of AR-97Q mice compared with those of AR-24Q mice (Supplementary Material, Fig. S1B and D). This increase was comparable to that seen in anti-GFP immunohistochemical staining (Supplementary Material, Fig. S1A and E), indicating again that the increased protein is due to increased reporter mRNA and that UPS function in the motor neurons of AR-97Q mice is well preserved.

Expression of proteasomal mRNAs and proteins are preserved in AR-97Q mice

To verify the protein expression levels of proteasomal subunits in advanced stage AR-24Q and AR-97Q mice, immunoblot analyses with various anti-proteasomal subunit antibodies

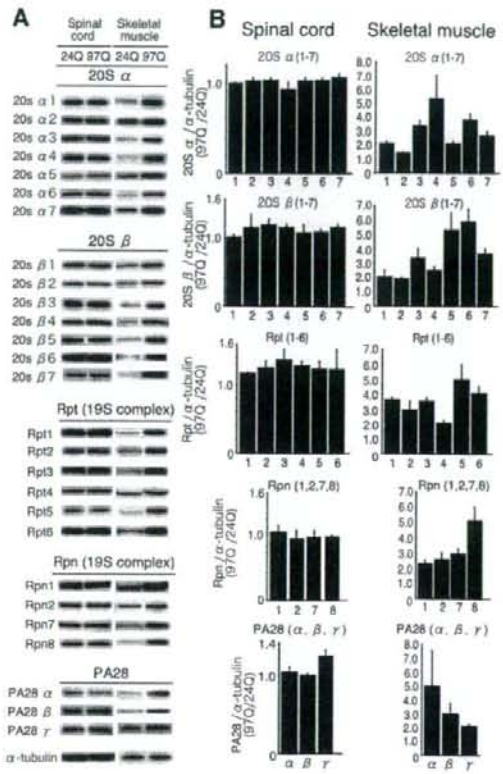

Figure 3. The protein expression levels of proteasome subunits in 16-week-old AR-97Q and AR-24Q mice. (**A**) Immunoblot analyses of various proteasome subunits in spinal cord and skeletal muscle. (**B**) Quantification of the ratios of subunit levels in AR-97Q versus AR-24Q mice.

were conducted in spinal cord and muscle lysates (Supplementary Material). The levels of all proteasome subunits, including those in the 20S proteasome (α1-7, β1-7), the 19S regulatory particles (Rpt1-6, Rpn1,2,7,8) and the proteasome activators (PA28α,β,γ) in the spinal cord of AR-97Q mice, were similar to those in the AR-24Q mice (Fig. 3A and B). On the other hand, protein levels of all proteasomal subunits in the skeletal muscle of the AR-97Q mice were higher than those in the AR-24Q mice (Fig. 3A and B). Representative immunohistochemical analyses also revealed the elevated expression levels of proteasomal subunits 20S α1, α4, α5, α7, β2 and 19S Rpt3 in the skeletal muscle of AR-97Q versus AR-24Q mice (Supplementary Material, Fig. S2) and no differences in the patterns of proteasomal subunit stainings in the spinal anterior horn cells of the AR-24Q and AR-97Q mice (Supplementary Material, Fig. S2). Likewise, quantitative real-time RT–PCR analysis showed that levels of mRNA encoding representative proteasomal subunits in the spinal cords of AR-97Q mice were similar to those in AR-24Q mice (Supplementary Material, Fig. S3A), whereas mRNA levels of the same proteasomal subunits were

increased in AR-97Q skeletal muscle compared with AR-24Q (Supplementary Material, Fig. S3B). Thus, the increases in proteasomal subunit mRNAs were well correlated to those in proteasomal subunit proteins, to increased chymotryptic activity and to ubiquitin-dependent degradation of ^{35}S-labeled cIAP1 in AR-97Q skeletal muscle. Furthermore, there was no difference in the proteasomal subunit expression levels in the spinal anterior horn cells of the AR-24Q and AR-97Q mice. Next we evaluated the co-localization of proteasomal subunits and mutant AR in AR-97Q mice. Double-immunofluorescence staining with anti-20S proteasome α1 or α7 subunit and mouse anti-expanded polyQ (1C2) antibodies revealed that the 20S proteasome α1 or α7 subunits (Supplementary Material, Fig. S4A, D, G and J) and mutant AR (Supplementary Material, Fig. S4B, E, H and K) were partially co-localized in the nuclei (Supplementary Material, Fig. S4C, F, I and L) of the spinal anterior horn neurons and skeletal muscle cells of the AR-97Q mice, suggesting that the proteasomal subunits co-exist with mutant AR and exert their function in the AR-97Q mice. Moreover, the expression levels of 20S proteasome α1 and α7 subunits appeared to be elevated in the 1C2-positive muscle fibers (Supplementary Material, Fig. S4I and L), and those signals were unchanged in spinal motor neurons (Supplementary Material, Fig. S4A–F), indicating that the increase observed in the skeletal muscle is due to direct effects of the mutant AR on the skeletal muscle. Taken together, the results demonstrate there was no significant impairment of UPS activity in the AR-97Q mice with severe phenotypes.

17-DMAG preferentially reduces the amount of the polyQ-expanded mutant AR by integrating into the Hsp90 chaperone complex

To examine the efficacy of 17-DMAG to degrade mutant polyQ-expanded AR, we treated SH-SY5Y cells highly expressing either AR-24Q or AR-97Q with 17-DMAG or vehicle (DMSO). Although the anti-AR immunoblot showed a dose-dependent decline in both wild-type and mutant AR expression in response to 17-DMAG (Fig. 4A), the decrease in monomeric mutant AR (70% at 100 nM 17-DMAG) was significantly more than in wild-type (29%; Fig. 4B), suggesting that mutant AR is more selectively degraded by 17-DMAG than is wild-type. In addition, the pharmacological effect of 17-DMAG was three times as strong as that of 17-AAG (Fig. 4C and D). 17-DMAG also significantly increased the expression of both Hsp70 and Hsp40, but only slightly increased Hsp90 expression (Fig. 4A and B). There were no significant differences, however, in the levels of Hsp70 and Hsp40 induction in cells transfected with the wild-type or mutant AR (Fig. 4B). There was also no difference in cell viability between wild-type- and mutant AR-transfected cells (data not shown). These data indicate that 17-DMAG preferentially degrades the mutant AR protein without cellular toxicity.

We next examined the status of the Hsp90 chaperone complex in mutant AR-expressing cultured cells treated with 17-DMAG. After 30 min of 17-DMAG treatment, immunoprecipitation with an AR-specific antibody showed that Hsp90 chaperone complex-associated Hop was markedly increased and p23 decreased in a dose-dependent manner (Fig. 4E), suggesting that treatment with 17-DMAG shifted the AR-Hsp90 chaperone complex from a mature stabilizing form with p23 to a proteasome-targeting form with Hop (33). This finding is consistent with our previous report using 17-AAG (11). Immunoprecipitation with the AR-specific antibody showed that the mutant AR was more strongly ubiquitinated in cells treated with 17-DMAG in the presence of the proteasome inhibitor MG132 than those treated with DMSO alone (Fig. 4F). In addition, the degradation of mutant AR-97Q by 17-DMAG was completely suppressed by MG132 (Fig. 4F, bottom row). These results suggest that following treatment with 17-DMAG, the Hsp90 chaperone complex and client proteins are targeted for degradation via the UPS as previously reported (34,35).

The mutant AR was shown to be degraded only when Hsp70 was induced (36). However, mutant AR was markedly decreased following treatment with 17-DMAG, even when the induction of Hsp70 was blocked by a small interfering RNA (Fig. 4G and H). This suggests that 17-DMAG contributes to the preferential degradation of mutant AR through Hsp90 chaperone complex formation and subsequent proteasome-dependent degradation, even without induction of Hsp70.

17-DMAG ameliorates phenotypic expression of the SBMA transgenic mouse

We administrated 17-DMAG from age 5 to 25 weeks at doses of 1.0 or 10 mg/kg to male AR-97Q or AR-24Q mice and examined various neurological and behavioral parameters. The disease progression of AR-97Q mice treated with 10 mg/kg 17-DMAG (Tg-10) was significantly ameliorated and that of mice treated with 1.0 mg/kg 17-DMAG (Tg-1) mildly ameliorated (Fig. 5A–D). The untreated male mice (Tg-0) showed motor impairment assessed by the Rotarod task as early as 9 weeks after birth, whereas the Tg-10 mice showed initial impairment only 16 weeks after birth and with less deterioration than the Tg-0 mice ($P<0.005$, Fig. 5A). The locomotor cage activity of the Tg-0 mice was also significantly decreased at 10 weeks compared with the Tg-10 mice ($P < 0.005$, Fig. 5B). The Tg-0 mice lost weight significantly earlier and more profoundly than the Tg-10 mice ($P < 0.005$, Fig. 5C). 17-DMAG also significantly prolonged the survival rate of both the Tg-1 ($P < 0.05$) and Tg-10 ($P < 0.0001$) mice compared with the Tg-0 mice (Fig. 5D). Although both the Tg-10 and Tg-1 mice showed ameliorated phenotypic expressions, the Tg-10 mice were better than the Tg-1 mice in all parameters, suggesting that the improved motor phenotype depended on drug efficacy. In addition, the Tg-0 mice showed motor weakness, taking shorter steps and dragging their legs, whereas the Tg-10 mice showed almost normal ambulation (Fig. 5E and F).

To evaluate the toxicity of 17-DMAG, we examined blood samples from 25-week-old mice treated with 10 mg/kg 17-DMAG for 20 weeks (Supplementary Material). Measurements of aspartate aminotransferase, alanine aminotransferase, blood urea nitrogen and serum creatinine demonstrated that 17-DMAG resulted in neither liver nor renal dysfunction in the AR-97Q mice at the dose of 10 mg/kg (Supplementary Material, Fig. S5). Additionally, no treated mice were infertile (data not shown).

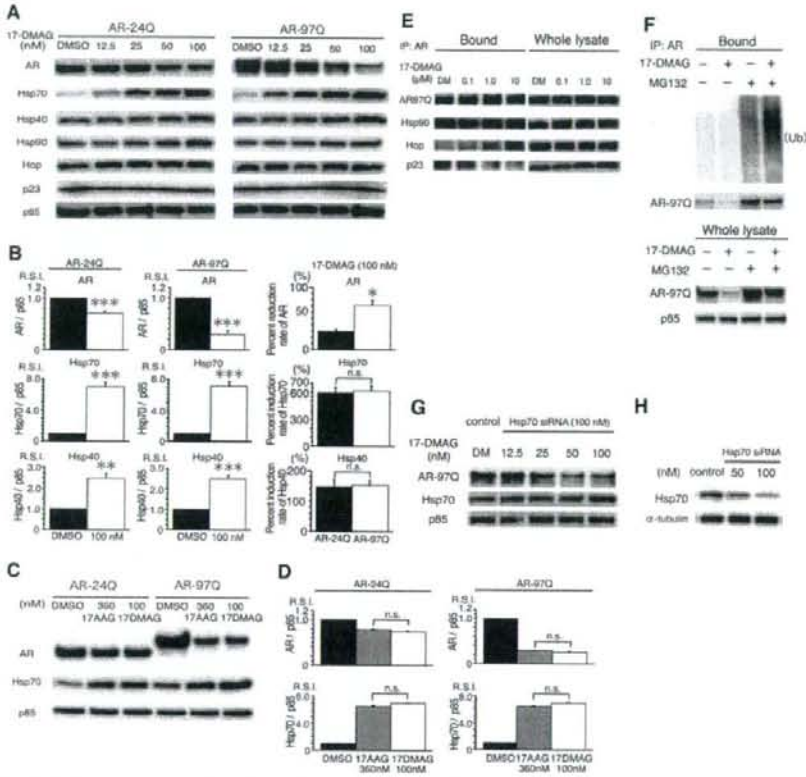

Figure 4. Effect of 17-DMAG on expression levels of AR or chaperones and on ubiquitination of AR in cultured cells. (**A**) Immunoblots of AR and chaperone proteins from transfected SH-SY5Y cells highly expressing the wild-type (AR-24Q) or mutant (AR-97Q) AR and treated with the indicated doses of 17-DMAG or with the vehicle DMSO. p85 was used as a loading control. (**B**) Densitometric analyses of AR, Hsp70 and Hsp40 in vehicle (DMSO) and 17-DMAG (100 nM) treated SH-SY5Y cells expressing the wild-type (AR-24Q) or mutant (AR-97Q) AR. Values are expressed as mean ± SE, $n = 5$; $^{*}P < 0.005$; $^{**}P < 0.0005$; $^{***}P < 0.0001$. (**C**) Western blot analysis of AR and Hsp70 proteins in SH-SY5Y cells expressing AR-24Q or AR-97Q following treatment with the indicated doses of 17-AAG, 17-DMAG or with the vehicle DMSO. (**D**) Densitometric analyses of AR and Hsp70 in vehicle (DMSO), 17-AAG (360 nM) and 17-DMAG (100 nM) treated SH-SY5Y cells expressing AR-24Q or AR-97Q. The decreases in both ARs and the induction of Hsp70 expression following 17-AAG or 17-DMAG were similar, but the concentration of 17-AAG was more than three times that of 17-DMAG. Values are expressed as mean ± SE, $n = 5$. (**E**) Pharmacological changes in the AR-Hsp90 complex. Transfected cells expressing mutant AR were treated with the indicated doses of 17-DMAG or DMSO (DM) for 30 min, immunoprecipitated with an anti-AR antibody and then immunoblotted with antibodies against the indicated Hsp90 chaperone complex proteins and client proteins. Note that the short time exposure to 17-DMAG did not decrease the amount of mutant AR. (**F**) Effect of 17-DMAG, in the presence of the proteasome inhibitor MG132, on ubiquitination and AR expression. (**G**) Immunoblot showing the effects of 17-DMAG or DMSO (DM) on the expression of mutant AR when Hsp70 induction was inhibited by siRNA. (**H**) Western blot analysis of endogenous Hsp70 protein expression from SH-SY5Y cells exposed to the control oligonucleotide or indicated concentrations of siRNA for 48 h.

17-DMAG preferentially degrades mutant AR protein and significantly increases Hsp70 and Hsp40 in SBMA mice

Treatment with 17-DMAG significantly diminished both the high-molecular-weight complex and the monomeric mutant AR in the spinal cord and muscle of AR-97Q mice ($P < 0.05$), but only slightly diminished the wild-type monomeric AR in AR-24Q mice (Fig. 6A and B). In the AR-97Q mice, monomeric AR decreased by 71% in the spinal cord and 70% in the skeletal muscle, but only by 37 and 27%, respectively, in the AR-24Q mice (Fig. 6A and B). RT–PCR in both AR-24Q and AR-97Q mice showed that the levels of AR mRNA were similar in the treated (Tg-10) and untreated (Tg-0) mice (Supplementary Material, Fig. S6), implying that the decreased protein was due to degradation and not to lower mRNA levels. We also conducted filter-trap assays (Supplementary Material) for both the large molecular weight aggregated and the soluble forms of mutant AR. Both forms of trapped AR-97Q protein were markedly reduced in the spinal cord and muscle of treated mice (Supplementary Material, Fig. S7). These observations indicate that 17-DMAG preferentially degrades not only the

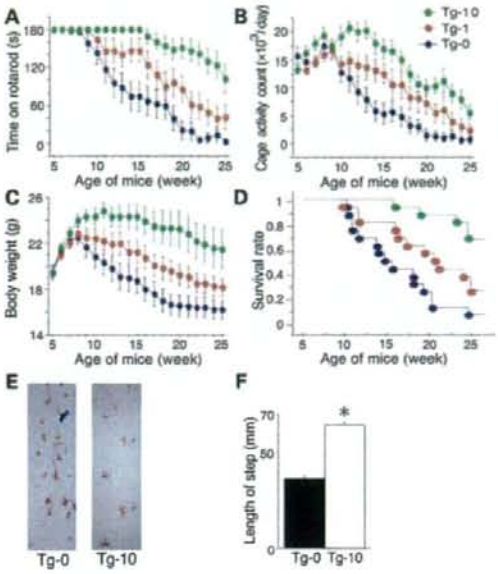

Figure 5. Effects of 17-DMAG on behavioral phenotypes in male AR-97Q mice. (**A–D**) Untreated mice (Tg-0) or those administered 1 (Tg-1) or 10 mg/kg (Tg-10) 17-DMAG from age 5 to 25 weeks were tested on the Rotarod task (A) for cage activity (B) and body weight (C). All parameters were significantly different between the Tg-0 and Tg-10 mice ($P < 0.005$ for all parameters, $n = 16$). (D) A Kaplan–Meier plot shows the prolonged survival of the Tg-1 and Tg-10 mice compared with the Tg-0 mice; $P < 0.05$; $P < 0.0001$, respectively. (**E**) Footprints of representative 16-week-old Tg-0 and Tg-10 mice. Front paws are indicated in red, and hind paws are in blue. (**F**) The length of steps was measured in 16-week-old Tg-0 and Tg-10 mice. Each column shows the average length of steps of the hind paw. Values are expressed as mean ± SE, $n = 5$; $^*P < 0.0001$.

high-molecular-weight mutant AR complex but also the monomeric mutant AR protein.

17-DMAG treatment of transgenic mice was also accompanied by marked chaperone induction. The levels of Hsp70 and Hsp40 in the spinal cord were increased by 367 ($P < 0.005$) and 105% ($P < 0.0001$), respectively, and in the muscle by 235 ($P < 0.05$) and 195% ($P < 0.0001$), respectively (Fig. 6C and D) following 17-DMAG treatment. These pharmacological effects of 17-DMAG on chaperone induction were more pronounced than those of 17-AAG in our previous study (11). The enhanced chaperone induction accompanying 17-DMAG treatment might be responsible for its enhanced pharmacological effect of reducing mutant AR.

Immunohistochemical staining for mutant AR showed a significant reduction in 1C2-positve diffuse nuclear staining and NIs in the spinal anterior horn (Fig. 6E) and skeletal muscle (Fig. 6F) in the Tg-10 mice (Fig. 6G). Anti-glial fibrillary acidic protein (GFAP) staining showed an apparent reduction in reactive astrogliosis in the Tg-10 mice in the spinal anterior horn (Fig. 6H). Muscle histology also demonstrated marked amelioration of muscle atrophy in the Tg-10 mice (Fig. 6I). AR-24Q mice and normal littermates treated with 17-DMAG displayed no altered phenotypes (data not shown).

DISCUSSION

The UPS is responsible for the turnover of most soluble proteins and plays an essential role in degrading short-lived regulatory proteins and damaged or misfolded proteins (37). We demonstrated that UPS activity during the advanced stage of SBMA model mice, assessed by chymotryptic activity and ubiquitin-dependent protein-degradation activity, was very well preserved in the spinal cord and even increased in the skeletal muscle. More importantly, the expression levels of 20S proteasome α1 and α7 subunits appeared to be elevated in the 1C2-positive muscle fibers (Supplementary Material, Fig. S4). In addition, UPS function semi-quantitatively evaluated in the GFP-based (Ub^{G76V}-GFP) reporter mouse (31) was also not impaired, data that are concordant with a previous study of an ataxia model of polyQ disease (25). Further evidence of preserved proteasomal function in the AR-97Q mice exhibiting advanced SBMA phenotypes is the data showing that protein levels of proteasome subunits in AR-97Q mice were similar to those in the AR-24Q mice in the spinal motor neurons and increased in skeletal muscle. Earlier studies of polyQ–mediated degeneration in cultured cell models (16,18,38), transgenic mice (39) and human postmortem samples (40) showed that components of the UPS are sequestrated in cellular aggregates or NIs, suggesting involvement of the UPS in polyQ diseases. The function of the UPS was evaluated in various assays that provided divergent results, ranging from impaired (19–21,24) to preserved (28,29) UPS function. It is possible that mutant polyQ-expanded proteins may directly affect proteasome function within the specific subcellular compartment of synaptic UPS activities (23), although it has been demonstrated that neuronal dysfunction can develop without significant impairment of the UPS in a mouse model of SCA7 (25). Consistent with this is data showing that proteasome impairment did not contribute to the pathogenesis of Huntington's disease in a mouse model (26). Furthermore, in conditional knockout mouse models of polyQ disease, genetic diminution of the abnormal gene led to rapid clearance of pre-existing polyQ aggregates and reversible improvement of abnormal phenotypes (41,42). If the UPS were irreversibly damaged in patients and animal models of polyQ diseases, then the aggregates of pathogenic proteins could not have been eliminated. Taking these data together, we considered that UPS function is well preserved in polyQ diseases, particularly in SBMA, and treatment with 17-DMAG, which enhances a self-clearing system of target disease-causing proteins via the UPS, is a reasonable therapeutic strategy against polyQ-related diseases. On the other hand, it is known that an age-dependent decrease in proteasome activity exists that may reduce the clearance of the misfolded proteins, resulting in their accumulation and contributing to late-onset polyQ-expanded toxicity. UPS-related genes were suppressed at the transcriptional level in the aged brain (43), and proteasome activity was also decreased in the aged brain (27,44), although brain proteasome activity was not specifically altered in the brains of Huntington's disease knock-in mice when compared with age-matched wild-type mice (27). As proteasome activity generally decreases in the central nervous system in aged animals (27,44), such an age-dependent decrease in UPS function is

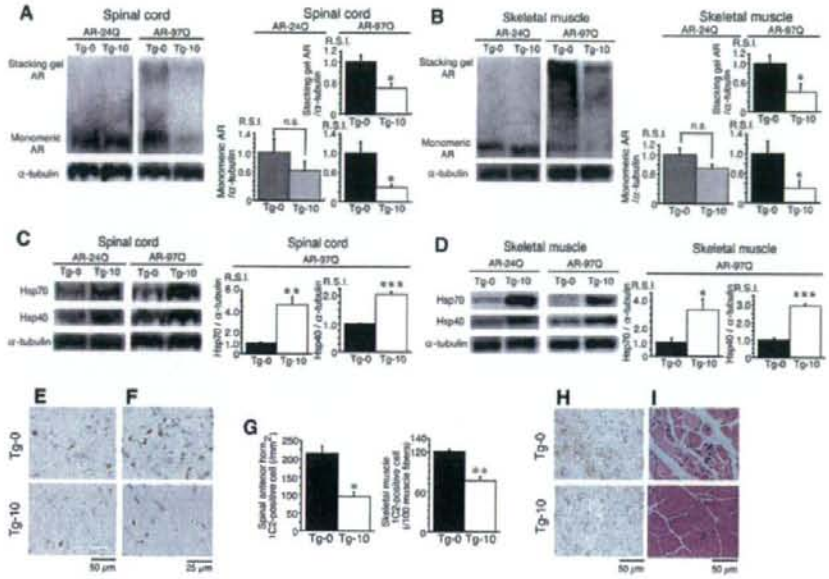

Figure 6. Effects of 17-DMAG on AR expression and histopathology in male AR-24Q and AE-97Q mice. (**A** and **B**) Western blot analyses (left) and image analysis quantification (right) of high-molecular-weight complex AR (in stacking gel) and monomeric mutant AR in the spinal cord (A) and muscle (B) of AR-24Q and AR-97Q mice probed with an AR-specific antibody. Values are expressed as mean ± SE, $n = 5$; $^{*}P < 0.05$. (**C** and **D**) Western blot analyses (left) and image analysis quantification (right) in the spinal cord (C) and muscle (D) of AR-24Q and AR-97Q mice probed with antibodies specific for the expression levels of Hsp70 and Hsp40. Values are expressed as mean ± SE, n=5. Statistical differences are indicated by asterisks; $^{*}P < 0.05$; $^{**}P < 0.005$; $^{***}P < 0.0001$. (**E** and **F**) Effects of 17-DMAG on the histopathology of male AR-97Q mice. Immunohistochemical staining with the 1C2 antibody, specific for mutant AR, showed marked differences in diffuse nuclear staining and NIs between Tg-0 and Tg-10 mice in the spinal anterior horn (E) and skeletal muscle (F). (**G**) Quantification of the number of 1C2-positive cells in the spinal cord and skeletal muscle in Tg-0 and Tg-10 mice. Values are expressed as mean ± SE, $n = 5$; $^{*}P < 0.005$; $^{**}P < 0.0005$. (**H**) Immunohistochemical staining with a GFAP-specific antibody shows reactive astrogliosis in the spinal anterior horn of untreated (Tg-0) mice and those treated with 17-DMAG. (**I**) Hematoxylin and eosin staining of the skeletal muscle in Tg-0 mice shows obvious grouped atrophy and small angulated fibers, not seen in Tg-10 mice.

unlikely to critically contribute to the region-specific neuropathology seen in different types of polyQ diseases.

We present a potent strategy for SBMA therapy, with 17-DMAG acting via a preserved or elevated proteasome activity. 17-DMAG has two major activities, preferential client protein degradation and Hsp induction; the present study revealed that polyQ-expanded mutant AR was preferentially degraded by treatment with 17-DMAG. Mutant AR elimination was mediated through its preferential incorporation into the Hsp90-chaperone complex (11,45), where it is prone to proteasomal degradation. Our present results in a transgenic mouse model also confirmed that 17-DMAG passes through the blood-brain barrier as previously reported (46) and that it demonstrates sufficient pharmacological effects in the central nervous system. We have already examined the effectiveness of 17-AAG in a mouse model of SBMA (11). 17-AAG has less toxicity (47) and higher selectivity (45) for client oncoproteins than does geldanamycin (48). 17-DMAG has a potential advantage over 17-AAG because its aqueous solubility eliminates the need for complicated formulations used to administer 17-AAG, and 17-DMAG induced the up-regulation of Hsp70 more than 17-AAG did (49). In a mouse study, the bioavailability of 17-DMAG by oral administration was twice that of orally delivered 17-AAG (46). Data from preclinical toxicity studies for 17-DMAG in animal models have recently become available (50) and phase I clinical trials for cancer are currently being performed (51,52). In addition, 17-DMAG is not metabolized to the potentially toxic metabolites that arise from CYP3A-mediated metabolism of the 17-allyl side chain of 17-AAG (14,46,53), indicating that 17-DMAG has less toxic side effects than 17-AAG. In fact, 17-DMAG shows greater oral bioavailability than 17-AAG, the pharmacological effect of 17-DMAG for mutant AR degradation was three times that of 17-AAG (Fig. 4C and D), and the inductions of Hsp70 and Hsp40 with 17-DMAG were more pronounced than with 17-AAG in the SBMA mouse model (Fig. 6C and D) (11). Moreover, the concentration necessary to obtain a similar therapeutic efficacy using 17-DMAG (10 mg/kg) was much lower than that using 17-AAG (25 mg/kg) (Fig. 5A–D) (11). Although 17-DMAG passes through the blood-brain barrier less than 17-AAG *in vivo* (14,46), these data show that 17-DMAG has more potent effects than 17-AAG.

Hsp90 inhibitors also function as Hsp inducers (54,55), resulting in the dissociation of HSF-1 from the Hsp90 complex and subsequent HSF-1 trimerization, thereby leading to Hsp activation (11). In this study, the inductions of Hsp70 and Hsp40 with 17-DMAG were more pronounced than with

17-AAG in our previous study (11). Hsps, particularly Hsp70, were shown to suppress aggregate formation and cellular toxicity in polyQ disease models (9,16,56). Hsp70 over-expression also enhanced degradation of polyQ-expanded proteins via its interaction with the UPS (36,57). CHIP (carboxyl terminus of Hsc70-interacting protein) might be one such coupling factor between the Hsp70 chaperone system and the machinery responsible for degrading mutant proteins (58,59). Thus, enhancement of chaperone expression using Hsp90 inhibitors under preserved UPS function is a further reasonable clinical approach for the treatment of pathogenic mutant or modified protein-mediated neurodegenerative diseases.

In conclusion, we have demonstrated that UPS function was well preserved or even enhanced in an SBMA model mouse and that 17-DMAG exerted potent therapeutic effects on the SBMA phenotype. In the case of other neurodegenerative diseases, phosphorylated tau would be one of the target proteins of Hsp90 inhibitors (60). Hsp90 inhibitors have also been shown to be effective in animal models of Parkinson's disease (61), stroke (62) and autoimmune encephalomyelitis (63). The combined therapy of 17-DMAG and leuprorelin would be expected to be more effective than the monotherapy with either 17-DMAG or leuprorelin (64), because the target sites of the agents are different and thus the therapeutic effect of the combined therapy would theoretically be additive or synergistic. 17-DMAG, by directly reducing disease-causing protein, presents a new therapeutic avenue for SBMA and has potentially widespread applications for other neurodegenerative diseases, particularly if the disease-causing protein belongs to the Hsp90 client protein family.

MATERIALS AND METHODS

DNA transfection

Full-length *AR* cDNAs were constructed by subcloning *AR* inserts into the pCR3.1 mammalian expression vector (Invitrogen) (11). SH-SY5Y cells were plated in 6 cm dishes in 5 ml of DMEM/F12 containing 10% fetal bovine serum with penicillin and streptomycin, and each dish was transfected with 8 μg of vector containing AR24, AR97 or mock (negative control) constructs using OPTI-MEM (Invitrogen) and Lipofectamine 2000 (Invitrogen) according to the manufacturer's instructions. The cells were cultured for 48 h at 37°C under 5% CO_2. Transfection efficiency was 60–70% in both AR-24Q and AR-97Q transfected cells, and no difference in transfection efficiencies was found. In this culture system, we detected a band of monomeric mutant AR in the separating gel, but barely detected the high-molecular-weight mutant AR protein complex, which was retained in the stacking gel. Therefore, this cultured cell model is better suited for estimating changes in monomeric mutant AR expression.

Therapeutic agents and protocol for administration

17-DMAG (NSC707545) was obtained from the Regulatory Affairs Branch, Division of Cancer Treatment and Diagnosis, National Cancer Institute (Bethesda, MD, USA) and Kosan Biosciences (Hayward, CA, USA). For cultured cell models, a 1 mM stock solution of 17-DMAG in DMSO was diluted into fresh medium to give final concentrations of 12.5–100 nM and added to the washed cells 24 h after transfection. Control cells were treated with DMSO alone. To show obvious pharmacological changes in the AR-Hsp90 complex, as demonstrated in a previous report (11), we exposed cultured cells to 17-DMAG for 30 min at concentrations of 0.1, 1.0 and 10 μM, 48 h after transfection.

For transgenic mice, the dosing solutions of 17-DMAG in saline were freshly prepared weekly. 17-DMAG treatments were started when mice were 5 weeks old and were continued until they were 16 weeks (or 25 weeks for toxicity studies). An optimal dose of 17-DMAG was determined based on a previous study in mice (50). Male AR-24Q and AR-97Q mice received 0.2 ml oral administration of 1 or 10 mg/kg 17-DMAG three times a week on alternate days; control mice received saline alone. Members of the same litter were distributed among the three treatment groups and homogeneities of body weight variances and means among the three groups were confirmed using Bartlett's test and one-way ANOVA.

Assay of proteasome activity

Mouse tissue homogenates from the spinal cord and muscle of 16-week-old AR-24Q and AR-97Q mice were clarified by centrifugation at 15 000 *g* and subjected to 8–32% (v/v) linear glycerol density gradient centrifugation (22 h, 83 000g). Proteasome chymotrypsin-like peptidase activity was measured using the peptide substrate, succinyl-Leu-Leu-Val-Tyr-7-amino-4-methyl-coumarin in the absence (i.e. 26S proteasome) of 0.025% sodium dodecyl sulfate (SDS) as described previously (65). For the assay of cIAP1 (inhibitor of apoptosis-1) degradation, cDNAs encoding Flag-cIAP1 subcloned into pcDNA3.1 were transcribed *in vitro*, translated and radiolabeled. The 35S-labeled Flag-cIAP1 was purified using M2-agarose (Sigma) and eluted with Flag-peptide (Sigma). The results were confirmed by duplicate measurements of the samples from different mice. For ubiquitination of cIAP1, 3 000 000 c.p.m. of 35S-labeled cIAP1, 0.25 μg of E1, 0.9 μg of UbcH5 and 33 μg of ubiquitin (Sigma) were mixed and incubated in a volume of 80 μl for 90 min at 30°C, as described previously (66). Finally, 2.5 ml of the ubiquitination mixture was added to 10 μl of cell lysate in the presence of 2 mM ATP, incubated at 37°C for 20 min and then radioactivities of trichloroacetic acid-soluble fractions were measured.

Generation and maintenance of TG mice and genotyping

We crossed the mice expressing full-length human AR with 24- (AR-24Q mice, 5-5 line) or 97-polyQ tracts (AR-97Q mice, 7-8 line) with Ub^{G76V}-GFP/1 line. The Ub^{G76V}-GFP/1 line was obtained from Dr Nico P. Dantuma in the Department of Cell and Molecular Biology, Karolinska Institute, and maintained in the B6 background. We screened mouse-tail DNA by PCR for the presence of the transgene using the primer sets as described previously (30,31).

Neurological and behavioral assessment of SBMA model mice

The AR-24Q and AR-97Q mice were generated and maintained as previously described (67). The AR-97Q male mice showed

progressive muscular atrophy and weakness as well as diffuse nuclear staining and NIs consisting of mutant AR. These phenotypes were very pronounced in male transgenic mice similar to SBMA patients (30). All animal experiments were performed in accordance with the National Institutes of Health Guide for the Care and Use of Laboratory Animals and under the approval of the Nagoya University Animal Experiment Committee. The mouse Rotarod task was performed using an Economex Rotarod (Ugo Basile), and cage activity was measured with the AB system (BrainScience Idea Osaka, Japan) as described previously (30,68). The investigators in the behavioral assessment were blinded to the treatments.

Protein expression analysis

Cells were lysed in CelLytic-M Mammalian Cell Lysis/Extraction Reagent (Sigma) with 1 mM PMSF and 6 μg/ml aprotinine and centrifuged at 15 000*g* for 15 min at 4°C, 48 h after transfection. Sixteen-week-old mice were exsanguinated under ketamine–xylazine anesthesia 12 h after the final treatment of 17-DMAG, and tissues were snap-frozen with powdered CO_2 in acetone. The tissues were homogenized in CelLytic-M Mammalian Cell Lysis/Extraction Reagent (Sigma) with 1 mM PMSF and 6 μg/ml aprotinine and centrifuged at 2500*g* for 15 min at 4°C. Supernatant fraction protein concentrations were determined using the DC protein assay (Bio-Rad). Aliquots of supernatant fractions were loaded on 5–20% SDS–PAGE gels, each lane containing 7 μg protein for cells, 160 μg for nervous tissue and 80 μg for muscular tissue, and then transferred to Hybond-P membranes (GE Healthcare) using 25 mM Tris, 192 mM glycine, 0.1% SDS and 10% methanol as transfer buffer. Primary antibodies were used at the following concentrations: rabbit anti-AR (1:1000, H280; Santa Cruz or 1:1000, N-20; Santa Cruz); mouse anti-Hsp70 (1:1000, SPA-810; Assay Designs); rabbit anti-Hsp40 (1:5000, SPA-400; Assay Designs); mouse anti-Hsp90 (1:1000, F-8; Santa Cruz); mouse anti-Hop (1:1000, SRA-1500; Assay Designs); mouse anti-p23 (1:1000, MA3-414; Affinity BioReagents); rabbit anti-p85 (1:2000, Upstate); and mouse anti-α-tubulin (1:5000, T9026; Sigma); mouse anti-GFP (1:5000, MAB3580; Millipore); anti-20S proteasome subunits α3, α4, α5 and α6 (Biomol); anti-20S proteasome subunits β2, β3, β4, β5i, β6 and β7 (Biomol); anti-19S proteasome subunits Rpt1, Rpt2, Rpt3, Rpt4, Rpt5 and Rpt6 (Biomol); rabbit anti-11S proteasome regulator (PA28) PA28α, PA28β, PA28γ subunits (Biomol); rabbit anti-20S proteasome α1, α2, α7, β1; mouse anti-19S proteasome subunit Rpn2; and rabbit anti-19S proteasome subunits Rpn1, Rpn7, Rpn8 (1:1000) (65,69,70). Primary antibodies were probed using HRP-conjugated anti-rabbit Ig F $(ab')_2$ and anti-mouse Ig F $(ab')_2$ (1:5000, GE Healthcare) secondary antibodies and detected with the ECL+plus kit (GE Healthcare). An LAS-3000 imaging system was used to produce digital images and to quantify band intensities, which were then analyzed with Image Gauge software version 4.22 (Fujifilm, Tokyo, Japan). Densitometric values of AR, Hsp70, Hsp40 and GFP were normalized to those of endogenous p85 or α-tubulin. Relative signal intensity (RSI) was computed as the signal intensity of each sample divided by that of the Tg-0 mice (Fig. 6) or the 24Q/GFP mice (Fig. 2).

Immunoprecipitation from cultured cells was performed using 300 μg total protein lysate from cells, 10 μl Protein G Sepharose (GE Healthcare) and 5 μl anti-AR antibody (N-20; Santa Cruz). For experiments involving co-precipitation of AR, cells were lysed in molybdate-containing lysis buffer (10 mM Tris pH 7.4, 10 mM monothioglycerol, 10 mM Na_2MoO_4, 10 mM $MgCl_2$, 0.2% Tween-20, 1 mM PMSF and 6 μg/ml aprotinine). For the AR ubiquitination assay, a full-length AR was constructed by subcloning AR inserts derived from pCR-AR97 (97 CAG repeats) into the pDsRed monomer mammalian expression vector (Takara Bio, Otsu, Japan) (59). SH-SY5Y cells were seeded onto 60-mm plates and transfected with plasmids encoding DsRed-AR97 for a 48 h period. Cells were exposed to MG132 (20 μM) for a 1 h period and to MG132 (20 μM) and 17-DMAG (10 μM) for a 4 h period. Extracts were prepared and AR was immunoprecipitated with anti-DsRed antibody. Blots were probed with ubiquitin (1B3; MBL) and AR (N20; Santa Cruz) antibody.

Filter-trap assay

To quantify the large-molecular aggregated and soluble form of the mutant AR protein, filter-trap assays of total tissue homogenates from the spinal cord and muscle of male AR-24Q or AR-97Q mice (16 weeks old) were performed as previously described (36). Filtration of proteins through a 0.2 μm cellulose acetate membrane (Sartorius AG) was performed using a slot-blot apparatus (Bio-Rad). Only the larger-sized mutant AR protein was retained on the cellulose acetate membrane (pore 0.2 μm in diameter), whereas the nitrocellulose membrane captured protein of all sizes. In each case, the nitrocellulose membrane was placed under the cellulose acetate membrane to capture the soluble AR protein passing through this membrane. The membranes, supported by two pieces of filter paper (Bio-Rad), were washed three times with TBS buffer. Samples of protein, 200 μg for the spinal cord and 80 μg for the muscle, were prepared in a final volume of 200 μl lysis buffer, loaded and gently vacuumed. Membranes were washed three times with TBS containing 0.05% Tween-20. Slot-blots were probed as described for western blots by an antibody against AR (H-280; Santa Cruz) or α-tubulin (T9026; Sigma).

Quantitative real-time RT–PCR

The levels of AR and proteasomal subunit mRNAs were determined by real-time RT–PCR as described previously (11). Total RNA was isolated from SH-SY5Y cells using the RNeasy Mini Kit (QIAGEN) and from transgenic mouse spinal cord and muscle by homogenizing in Trizol (Invitrogen) according to the manufacturer's instructions. Total RNA (5 μg) from cells and mouse spinal cord and muscle were reverse transcribed using SuperScript III reverse transcriptase (Invitrogen). PCR primers were designed to amplify GFP cDNA sequences in GFP-reporter mouse tissues (5′-TATAT CATGGCCGACAAGCA and 5′-TGTTCTGCTGGTAGT GGTCG) (Fig. 2), proteasomal subunit cDNA sequences in mouse tissues (Psm a3: QT00168728, Psm a5: QT00137928, Psm a6: QT00124439, Psm b1: QT00121079, Psm b5: QT 00111216, Psm c5: QT00162022 and Psm e3: QT00167797)

(QIAGEN) (Supplementary Material, Fig. S3) and AR cDNA sequences in mouse tissues (5′-TTCCACACCCAGTGAAG C-3 and 5′-CCTGAGGAGTGAATTGATCC-3′) (Supplementary Material, Fig. S5). Real-time RT–PCR was carried out in a total volume of 50 μl, containing 25 μl of 2× QuantiTect SYBR Green PCR Master Mix (QIAGEN) and 10 μM of each primer. PCR products were detected by the iCycler system (Bio-Rad). The reaction conditions were 95°C for 15 min and then 45 cycles of 15 s at 94°C, 30 s at 55°C and 30 s at 72°C. As an internal standard control, the expression level of glyceraldehyde-3-phosphate dehydrogenase (GAPDH) was simultaneously quantified using the primers (5′-CTCAGAGGAG CCCAGATGA-3′ and 5′-GCTGGTCTTGCGGTACAGT-3′) for mouse tissues. RSI was computed as the signal intensity of each sample divided by that of the AR-24Q/GFP mice (Fig. 2), the AR-24Q mice (Supplementary Material, Fig. S3) or the Tg-0 mice (Supplementary Material, Fig. S5).

RNA interference

Oligonucleotide siRNA duplexes were synthesized by Takara Bio. siRNA sequences were as follows: scramble (control) siRNA, 5′-CAAUACUGAAGUAUCAACG-3′; Hsp70 siRNA, 5′-CGAAAGACAACAAUCUGUU-3′. Transfection was done using Lipofectamine 2000 (Invitrogen) according to the manufacturer's instructions. Hsp70 was efficiently downregulated upon siRNA exposure (Fig. 4H).

Cell viability assay

MTS-based cell proliferation assays were performed in triplicate using the CellTiter 96® AQueous One Solution Cell Proliferation Assay (Promega) 48 h after incubation with 17-DMAG.

Immunohistochemistry and histopathology

Mice were deeply anesthetized with ketamine–xylazine and transcardially perfused with 20 ml of 4% paraformaldehyde fixative in phosphate buffer (pH 7.4). Tissues were post-fixed overnight in 10% phosphate-buffered formalin and processed for paraffin embedding. At room temperature, 6 μm thick tissue sections were deparaffinized, dehydrated with alcohol and treated with formic acid for 5 min. The tissue sections were blocked with normal horse serum (1:20) and incubated with mouse anti-expanded polyQ antibody (1:10 000, 1C2; Millipore); mouse anti-GFAP antibody (1:1000, Boehringer Manheim Biochemica, Manheim, Germany); anti-20S proteasome subunits α4, α5, β2; anti-19S proteasome subunit Rpt3 (Biomol); and rabbit anti-20S proteasome α1 and α7. Primary antibodies were probed with a biotinylated anti-species specific IgG secondary antibodies (Vector Laboratories) and the immune complexes visualized using streptavidin-horseradish peroxidase (Dako) and 3,3′-diaminobenzidine as a substrate. Sections were counterstained with Mayer's hematoxylin. Paraffin-embedded, 6 μm thick sections of the gastrocnemius muscles were air-dried and stained with hematoxylin and eosin. Tissues from the GFP-reporter mice were post-fixed in 4% PFA in PBS (pH 7.4) for 16 h at 4°C. The tissues were immersed in a graded series of sucrose solutions in 0.01 M PBS at 4°C as follows: 3 h in 7% sucrose, 3 h in 14% sucrose and 16 h in 25% sucrose. The tissues were then embedded in Tissue-Tek OCT compound (Sakura Finetek) and frozen with powdered solid CO_2 in acetone (71). Because native GFP fluorescence was below the detection threshold in both the spinal cord and skeletal muscle, the expression of Ub^{G76V}-GFP was evaluated semi-quantitatively by immunohistochemistry with an anti-GFP antibody. Cryostat sections, 10 μm thick, were prepared from the frozen tissues and blocked with 5% goat serum, incubated with rabbit anti-GFP antibody (1:1000, NB600-308; Novus Biologicals) at 4°C overnight, and then incubated with Alexa 488-conjugated goat anti-rabbit IgG (1:1000; Invitrogen) at 4°C overnight. The stained sections were examined and photographed with a confocal laser scanning microscope (LSM 5 PASCAL; Carl Zeiss). To assess GFP-reporter expression levels in spinal anterior horn cells, immunohistochemistry signal intensities were quantified in at least 10 transverse sections from each mouse. Images of individual anterior horn cells on transverse sections of the spinal cord with signals for Ub^{G76V}-GFP reporter were captured at the desired magnification and stored with image software (Olympus, Tokyo, Japan). Levels of reporter in the images were quantitatively analyzed with image analysis software (WinROOF version 5, Mitani, Fukui, Japan). Signal intensities were expressed as individual intracellular signal levels of Ub^{G76V}-GFP reporter (arbitrary absorbance units) in spinal anterior horn cells by subtracting the mean background levels of three regions of interest in each section. For double-immunofluorescence staining of the spinal cord and skeletal muscle, sections were blocked with 5% normal goat serum and then sequentially incubated with anti-20S proteasome α1 or α7 subunit (1:200) and 1C2 antibody (1:10 000) at 4°C overnight. The sections were then incubated with Alexa 488-conjugated goat anti-rabbit IgG (1:1000; Molecular Probes) and Alexa 568-conjugated goat anti-mouse IgG (1:1000; Molecular Probes) for 8 h at 4°C. The stained sections were examined and photographed with a confocal laser scanning microscope (LSM 5 PASCAL; Carl Zeiss MicroImaging, Tokyo, Japan).

In situ hybridization

Formalin-fixed, paraffin-embedded 6 μm thick sections of spinal cord and skeletal muscle were processed for *in situ* hybridization using the Ventana Discovery system (Ventana) according to the manufacturer's instructions. GFP cDNA was obtained using the primers 5′-CCTGAAGTTCATCTGC ACCA-3′ and 5′- GTTCACCTTGATGCCGTTCT-3′. Digoxigenin-labeled cRNA antisense and sense probes of ~350 bp were generated for *in situ* hybridization from linearized plasmids for Ub^{G76V}-GFP reporter using Sp6 and T7 polymerases (Roche), respectively. No hybridization signal was observed with the sense probe for the expression of Ub^{G76V}-GFP reporter (data not shown). To assess gene expression levels in spinal anterior horn cells, signal intensities of *in situ* hybridization were quantified in at least 10 transverse sections from each mouse. Images of individual anterior horn cells on transverse sections of the spinal cord with signals for Ub^{G76V}-GFP reporter were captured at the desired magnification and stored with image software (Olympus). Signal levels of the images were

quantitatively analyzed with image analysis software (WinRoof version 5) and expressed as individual intracellular cytoplasmic signal levels (arbitrary absorbance units) of spinal anterior horn cells for Ub^{G76V}-GFP reporter by subtracting the mean background levels of three regions of interest in each section.

Quantification of 1C2-positive cells, glial cell reaction and muscle fiber size

For assessment of 1C2-positive cells, 6 μm thick coronal sections of the thoracic spinal cord and gastrocnemius muscle stained with 1C2 antibody (1:10 000, Millipore) were prepared and the number of 1C2-positive cells in each individual mouse was counted using a light microscope with a computer-assisted image analyzer (Luzex FS, Nikon, Tokyo, Japan). For assessment of 1C2-positive cells in the ventral horn of the spinal cord, 50 consecutive transverse sections of the thoracic spinal cord were prepared and 1C2-positive cells within the ventral horn of every fifth section were counted as described previously (64). Populations of 1C2-positive cells were expressed as the number per mm^2. For assessment of 1C2-positive cells in muscle, the number of 1C2-positive cells was calculated from counts of more than 500 fibers in randomly selected areas and expressed as the number per 100 muscle fibers. The quantitative data of six individual mice were expressed as mean ± SE.

Hematological examination

AST and ALT were measured by ultraviolet spectrophotometry, BUN by the Urease-GLDH UV assay and Cre by an enzyme assay (Mitsubishi Kagaku Bio-Clinical Laboratories, Tokyo, Japan).

Statistical analyses

Data were analyzed by unpaired *t*-tests in Figures 1B, 2, 4B, 4D, 5F and 6 and Supplementary Material, Figures S1, S3, S5 and S6 and Kaplan–Meier and log-rank tests for survival rate in Figure 5D using Statview software version 5 (HULINKS, Tokyo, Japan). Statistical significance of the drug–dose dependency of phenotypes in Figure 5A–C was examined by the Williams test for multiple comparisons using Microsoft Excel 2004 (Microsoft).

SUPPLEMENTARY MATERIAL

Supplementary Material is available at *HMG* online.

ACKNOWLEDGEMENTS

We thank the National Cancer Institute and Kosan Biosciences for kindly providing 17-DMAG, and Noboru Ogiso, Yasutaka Ohya and Kumiko Yano in the Division for Research of Laboratory Animals, Center for Research of Laboratory Animals and Medical Research Engineering for their technical assistances. We also thank Dr Nico P. Dantuma for kindly providing the Ub^{G76V}-GFP reporter mice.

Conflict of Interest statement. None declared.

FUNDING

This work was supported by a Center-of-Excellence (COE) grant and Grant-in-Aid for Scientific Research on Priority Areas (Research on Pathomechanisms of Brain Disorders) from Ministry of Education, Culture, Sports, Science and Technology of Japan and by Health and Labour Sciences Research Grants for research on psychiatric and neurological diseases and mental health from Ministry of Health, Labour and Welfare of Japan.

REFERENCES

1. Di Prospero, N.A. and Fischbeck, K.H. (2005) Therapeutics development for triplet repeat expansion diseases. *Nat. Rev. Genet.*, **6**, 756–765.
2. Adachi, H., Waza, M., Katsuno, M., Tanaka, F., Doyu, M. and Sobue, G. (2007) Pathogenesis and molecular targeted therapy of spinal and bulbar muscular atrophy. *Neuropathol. Appl. Neurobiol.*, **33**, 135–151.
3. Tanaka, F., Doyu, M., Ito, Y., Matsumoto, M., Mitsuma, T., Abe, K., Aoki, M., Itoyama, Y., Fischbeck, K.H. and Sobue, G. (1996) Founder effect in spinal and bulbar muscular atrophy (SBMA). *Hum. Mol. Genet.*, **5**, 1253–1257.
4. Sobue, G., Hashizume, Y., Mukai, E., Hirayama, M., Mitsuma, T. and Takahashi, A. (1989) X-linked recessive bulbospinal neuronopathy. A clinicopathological study. *Brain.* **112** (Pt 1), 209–232.
5. Adachi, H., Katsuno, M., Minamiyama, M., Waza, M., Sang, C., Nakagomi, Y., Kobayashi, Y., Tanaka, F., Doyu, M., Inukai, A. *et al.* (2005) Widespread nuclear and cytoplasmic accumulation of mutant androgen receptor in SBMA patients. *Brain*, **128**, 659–670.
6. Pratt, W.B. and Toft, D.O. (2003) Regulation of signaling protein function and trafficking by the hsp90/hsp70-based chaperone machinery. *Exp. Biol. Med. (Maywood)*, **228**, 111–133.
7. Poletti, A. (2004) The polyglutamine tract of androgen receptor: from functions to dysfunctions in motor neurons. *Front. Neuroendocrinol.*, **25**, 1–26.
8. Neckers, L. (2002) Heat shock protein 90 inhibition by 17-allylamino-17-demethoxygeldanamycin: a novel therapeutic approach for treating hormone-refractory prostate cancer. *Clin. Cancer Res.*, **8**, 962–966.
9. Muchowski, P.J. and Wacker, J.L. (2005) Modulation of neurodegeneration by molecular chaperones. *Nat. Rev. Neurosci.*, **6**, 11–22.
10. Workman, P., Burrows, F., Neckers, L. and Rosen, N. (2007) Drugging the cancer chaperone HSP90: combinatorial therapeutic exploitation of oncogene addiction and tumor stress. *Ann. N. Y. Acad. Sci.*, **1113**, 202–216.
11. Waza, M., Adachi, H., Katsuno, M., Minamiyama, M., Sang, C., Tanaka, F., Inukai, A., Doyu, M. and Sobue, G. (2005) 17-AAG, an Hsp90 inhibitor, ameliorates polyglutamine-mediated motor neuron degeneration. *Nat. Med.*, **11**, 1088–1095.
12. Smith, V., Sausville, E.A., Camalier, R.F., Fiebig, H.H. and Burger, A.M. (2005) Comparison of 17-dimethylaminoethylamino-17-demethoxy-geldanamycin (17DMAG) and 17-allylamino-17-demethoxygeldanamycin (17AAG) in vitro: effects on Hsp90 and client proteins in melanoma models. *Cancer Chemother. Pharmacol.*, **56**, 126–137.
13. Herbst, M. and Wanker, E.E. (2007) Small molecule inducers of heat-shock response reduce polyQ-mediated huntingtin aggregation. A possible therapeutic strategy. *Neurodegener. Dis.*, **4**, 254–260.
14. Egorin, M.J., Lagattuta, T.F., Hamburger, D.R., Covey, J.M., White, K.D., Musser, S.M. and Eiseman, J.L. (2002) Pharmacokinetics, tissue distribution, and metabolism of 17-(dimethylaminoethylamino)-17-demethoxygeldanamycin (NSC 707545) in CD2F1 mice and Fischer 344 rats. *Cancer Chemother. Pharmacol.*, **49**, 7–19.
15. La Spada, A.R. and Weydt, P. (2005) Targeting toxic proteins for turnover. *Nat. Med.*, **11**, 1052–1053.
16. Cummings, C.J., Mancini, M.A., Antalffy, B., DeFranco, D.B., Orr, H.T. and Zoghbi, H.Y. (1998) Chaperone suppression of aggregation and altered subcellular proteasome localization imply protein misfolding in SCA1. *Nat. Genet.*, **19**, 148–154.

17. Ciechanover, A. and Brundin, P. (2003) The ubiquitin proteasome system in neurodegenerative diseases: sometimes the chicken, sometimes the egg. *Neuron*, **40**, 427–446.
18. Bence, N.F., Sampat, R.M. and Kopito, R.R. (2001) Impairment of the ubiquitin-proteasome system by protein aggregation. *Science*, **292**, 1552–1555.
19. Jana, N.R., Zemskov, E.A., Wang, G. and Nukina, N. (2001) Altered proteasomal function due to the expression of polyglutamine-expanded truncated N-terminal huntingtin induces apoptosis by caspase activation through mitochondrial cytochrome c release. *Hum. Mol. Genet.*, **10**, 1049–1059.
20. Bennett, E.J., Bence, N.F., Jayakumar, R. and Kopito, R.R. (2005) Global impairment of the ubiquitin-proteasome system by nuclear or cytoplasmic protein aggregates precedes inclusion body formation. *Mol. Cell*, **17**, 351–365.
21. Bennett, E.J., Shaler, T.A., Woodman, B., Ryu, K.Y., Zaitseva, T.S., Becker, C.H., Bates, G.P., Schulman, H. and Kopito, R.R. (2007) Global changes to the ubiquitin system in Huntington's disease. *Nature*, **448**, 704–708.
22. Rusmini, P., Sau, D., Crippa, V., Palazzolo, I., Simonini, F., Onesto, E., Martini, L. and Poletti, A. (2007) Aggregation and proteasome: the case of elongated polyglutamine aggregation in spinal and bulbar muscular atrophy. *Neurobiol. Aging*, **28**, 1099–1111.
23. Wang, J., Wang, C.E., Orr, A., Tydlacka, S., Li, S.H. and Li, X.J. (2008) Impaired ubiquitin-proteasome system activity in the synapses of Huntington's disease mice. *J. Cell Biol.*, **180**, 1177–1189.
24. Seo, H., Sonntag, K.C. and Isacson, O. (2004) Generalized brain and skin proteasome inhibition in Huntington's disease. *Ann. Neurol.*, **56**, 319–328.
25. Bowman, A.B., Yoo, S.Y., Dantuma, N.P. and Zoghbi, H.Y. (2005) Neuronal dysfunction in a polyglutamine disease model occurs in the absence of ubiquitin-proteasome system impairment and inversely correlates with the degree of nuclear inclusion formation. *Hum. Mol. Genet.*, **14**, 679–691.
26. Bett, J.S., Goellner, G.M., Woodman, B., Pratt, G., Rechsteiner, M. and Bates, G.P. (2006) Proteasome impairment does not contribute to pathogenesis in R6/2 Huntington's disease mice: exclusion of proteasome activator REGgamma as a therapeutic target. *Hum. Mol. Genet.*, **15**, 33–44.
27. Zhou, H., Cao, F., Wang, Z., Yu, Z.X., Nguyen, H.P., Evans, J., Li, S.H. and Li, X.J. (2003) Huntingtin forms toxic NH2-terminal fragment complexes that are promoted by the age-dependent decrease in proteasome activity. *J. Cell Biol.*, **163**, 109–118.
28. Ding, Q., Lewis, J.J., Strum, K.M., Dimayuga, E., Bruce-Keller, A.J., Dunn, J.C. and Keller, J.N. (2002) Polyglutamine expansion, protein aggregation, proteasome activity, and neural survival. *J. Biol. Chem.*, **277**, 13935–13942.
29. Diaz-Hernandez, M., Hernandez, F., Martin-Aparicio, E., Gomez-Ramos, P., Moran, M.A., Castano, J.G., Ferrer, I., Avila, J. and Lucas, J.J. (2003) Neuronal induction of the immunoproteasome in Huntington's disease. *J. Neurosci.*, **23**, 11653–11661.
30. Katsuno, M., Adachi, H., Kume, A., Li, M., Nakagomi, Y., Niwa, H., Sang, C., Kobayashi, Y., Doyu, M. and Sobue, G. (2002) Testosterone reduction prevents phenotypic expression in a transgenic mouse model of spinal and bulbar muscular atrophy. *Neuron*, **35**, 843–854.
31. Lindsten, K., Menendez-Benito, V., Masucci, M.G. and Dantuma, N.P. (2003) A transgenic mouse model of the ubiquitin/proteasome system. *Nat. Biotechnol.*, **21**, 897–902.
32. Dantuma, N.P., Lindsten, K., Glas, R., Jellne, M. and Masucci, M.G. (2000) Short-lived green fluorescent proteins for quantifying ubiquitin/proteasome-dependent proteolysis in living cells. *Nat. Biotechnol.*, **18**, 538–543.
33. Whitesell, L. and Cook, P. (1996) Stable and specific binding of heat shock protein 90 by geldanamycin disrupts glucocorticoid receptor function in intact cells. *Mol. Endocrinol.*, **10**, 705–712.
34. Mimnaugh, E.G., Chavany, C. and Neckers, L. (1996) Polyubiquitination and proteasomal degradation of the p185c-erbB-2 receptor protein-tyrosine kinase induced by geldanamycin. *J. Biol. Chem.*, **271**, 22796–22801.
35. Bonvini, P., Dalla Rosa, H., Vignes, N. and Rosolen, A. (2004) Ubiquitination and proteasomal degradation of nucleophosmin-anaplastic lymphoma kinase induced by 17-allylamino-demethoxygeldanamycin: role of the co-chaperone carboxyl heat shock protein 70-interacting protein. *Cancer Res.*, **64**, 3256–3264.
36. Adachi, H., Katsuno, M., Minamiyama, M., Sang, C., Pagoulatos, G., Angelidis, C., Kusakabe, M., Yoshiki, A., Kobayashi, Y., Doyu, M. *et al.* (2003) Heat shock protein 70 chaperone overexpression ameliorates phenotypes of the spinal and bulbar muscular atrophy transgenic mouse model by reducing nuclear-localized mutant androgen receptor protein. *J. Neurosci.*, **23**, 2203–2211.
37. Hegde, A.N. and Upadhya, S.C. (2007) The ubiquitin-proteasome pathway in health and disease of the nervous system. *Trends Neurosci.*, **30**, 587–595.
38. Wyttenbach, A., Carmichael, J., Swartz, J., Furlong, R.A., Narain, Y., Rankin, J. and Rubinsztein, D.C. (2000) Effects of heat shock, heat shock protein 40 (HDJ-2), and proteasome inhibition on protein aggregation in cellular models of Huntington's disease. *Proc. Natl Acad. Sci. USA*, **97**, 2898–2903.
39. Davies, S.W., Turmaine, M., Cozens, B.A., DiFiglia, M., Sharp, A.H., Ross, C.A., Scherzinger, E., Wanker, E.E., Mangiarini, L. and Bates, G.P. (1997) Formation of neuronal intranuclear inclusions underlies the neurological dysfunction in mice transgenic for the HD mutation. *Cell*, **90**, 537–548.
40. DiFiglia, M., Sapp, E., Chase, K.O., Davies, S.W., Bates, G.P., Vonsattel, J.P. and Aronin, N. (1997) Aggregation of huntingtin in neuronal intranuclear inclusions and dystrophic neurites in brain. *Science*, **277**, 1990–1993.
41. Yamamoto, A., Lucas, J.J. and Hen, R. (2000) Reversal of neuropathology and motor dysfunction in a conditional model of Huntington's disease. *Cell*, **101**, 57–66.
42. Zu, T., Duvick, L.A., Kaytor, M.D., Berlinger, M.S., Zoghbi, H.Y., Clark, H.B. and Orr, H.T. (2004) Recovery from polyglutamine-induced neurodegeneration in conditional SCA1 transgenic mice. *J. Neurosci.*, **24**, 8853–8861.
43. Lee, C.K., Weindruch, R. and Prolla, T.A. (2000) Gene-expression profile of the ageing brain in mice. *Nat. Genet.*, **25**, 294–297.
44. Keller, J.N., Huang, F.F. and Markesbery, W.R. (2000) Decreased levels of proteasome activity and proteasome expression in aging spinal cord. *Neuroscience*, **98**, 149–156.
45. Kamal, A., Thao, L., Sensintaffar, J., Zhang, L., Boehm, M.F., Fritz, L.C. and Burrows, F.J. (2003) A high-affinity conformation of Hsp90 confers tumour selectivity on Hsp90 inhibitors. *Nature*, **425**, 407–410.
46. Egorin, M.J., Zuhowski, E.G., Rosen, D.M., Sentz, D.L., Covey, J.M. and Eiseman, J.L. (2001) Plasma pharmacokinetics and tissue distribution of 17-(allylamino)-17-demethoxygeldanamycin (NSC 330507) in CD2F1 mice1. *Cancer Chemother. Pharmacol.*, **47**, 291–302.
47. Page, J., Heath, J., Fulton, R., Yalkowsky, E., Tabibi, E., Tomaszewski, J., Smith, A. and Rodman, L. (1997) Comparison of geldanamycin (NSC-122750) and 17-allylaminogeldanamycin (NSC-330507D) toxicity in rats. *Proc. Am. Assoc. Cancer Res.*, **38**, 308.
48. Supko, J.G., Hickman, R.L., Grever, M.R. and Malspeis, L. (1995) Preclinical pharmacologic evaluation of geldanamycin as an antitumor agent. *Cancer Chemother. Pharmacol.*, **36**, 305–315.
49. Wetzler, M., Earp, J.C., Brady, M.T., Keng, M.K. and Jusko, W.J. (2007) Synergism between arsenic trioxide and heat shock protein 90 inhibitors on signal transducer and activator of transcription protein 3 activity—pharmacodynamic drug-drug interaction modeling. *Clin. Cancer Res.*, **13**, 2261–2270.
50. Hollingshead, M., Alley, M., Burger, A.M., Borgel, S., Pacula-Cox, C., Fiebig, H.H. and Sausville, E.A. (2005) In vivo antitumor efficacy of 17-DMAG (17-dimethylaminoethylamino-17-demethoxygeldanamycin hydrochloride), a water-soluble geldanamycin derivative. *Cancer Chemother. Pharmacol.*, **56**, 115–125.
51. Shadad, F.N. and Ramanathan, R.K. (2006) 17-dimethylaminoethylamino-17-demethoxygeldanamycin in patients with advanced-stage solid tumors and lymphoma: a phase I study. *Clin. Lymphoma Myeloma*, **6**, 500–501.
52. Smith, M.A., Morton, C.L., Phelps, D.A., Kolb, E.A., Lock, R., Carol, H., Reynolds, C.P., Maris, J.M., Keir, S.T., Wu, J. *et al.* (2008) Stage 1 testing and pharmacodynamic evaluation of the HSP90 inhibitor alvespimycin (17-DMAG, KOS-1022) by the pediatric preclinical testing program. *Pediatr. Blood Cancer*, **51**, 34–41.
53. Egorin, M.J., Rosen, D.M., Wolff, J.H., Callery, P.S., Musser, S.M. and Eiseman, J.L. (1998) Metabolism of 17-(allylamino)-17-demethoxygeldanamycin (NSC 330507) by murine and human hepatic preparations. *Cancer Res.*, **58**, 2385–2396.

54. Zhang, Y.Q. and Sarge, K.D. (2007) Celastrol inhibits polyglutamine aggregation and toxicity though induction of the heat shock response. *J. Mol. Med.*, **85**, 1421–1428.
55. Sittler, A., Lurz, R., Lueder, G., Priller, J., Lehrach, H., Hayer-Hartl, M.K., Hartl, F.U. and Wanker, E.E. (2001) Geldanamycin activates a heat shock response and inhibits huntingtin aggregation in a cell culture model of Huntington's disease. *Hum. Mol. Genet.*, **10**, 1307–1315.
56. Katsuno, M., Sang, C., Adachi, H., Minamiyama, M., Waza, M., Tanaka, F., Doyu, M. and Sobue, G. (2005) Pharmacological induction of heat-shock proteins alleviates polyglutamine-mediated motor neuron disease. *Proc. Natl Acad. Sci. USA*, **102**, 16801–16806.
57. Bailey, C.K., Andriola, I.F., Kampinga, H.H. and Merry, D.E. (2002) Molecular chaperones enhance the degradation of expanded polyglutamine repeat androgen receptor in a cellular model of spinal and bulbar muscular atrophy. *Hum. Mol. Genet.*, **11**, 515–523.
58. Al-Ramahi, I., Lam, Y.C., Chen, H.K., de Gouyon, B., Zhang, M., Perez, A.M., Branco, J., de Haro, M., Patterson, C., Zoghbi, H.Y. *et al.* (2006) CHIP protects from the neurotoxicity of expanded and wild-type ataxin-1 and promotes their ubiquitination and degradation. *J. Biol. Chem.*, **281**, 26714–26724.
59. Adachi, H., Waza, M., Tokui, K., Katsuno, M., Minamiyama, M., Tanaka, F., Doyu, M. and Sobue, G. (2007) CHIP overexpression reduces mutant androgen receptor protein and ameliorates phenotypes of the spinal and bulbar muscular atrophy transgenic mouse model. *J. Neurosci.*, **27**, 5115–5126.
60. Dickey, C.A., Kamal, A., Lundgren, K., Klosak, N., Bailey, R.M., Dunmore, J., Ash, P., Shoraka, S., Zlatkovic, J., Eckman, C.B. *et al.* (2007) The high-affinity HSP90-CHIP complex recognizes and selectively degrades phosphorylated tau client proteins. *J. Clin. Invest.*, **117**, 648–658.
61. Auluck, P.K. and Bonini, N.M. (2002) Pharmacological prevention of Parkinson disease in Drosophila. *Nat. Med.*, **8**, 1185–1186.
62. Lu, A., Ran, R., Parmentier-Batteur, S., Nee, A. and Sharp, F.R. (2002) Geldanamycin induces heat shock proteins in brain and protects against focal cerebral ischemia. *J. Neurochem.*, **81**, 355–364.
63. Murphy, P., Sharp, A., Shin, J., Gavrilyuk, V., Dello Russo, C., Weinberg, G., Sharp, F.R., Lu, A., Heneka, M.T. and Feinstein, D.L. (2002) Suppressive effects of ansamycins on inducible nitric oxide synthase expression and the development of experimental autoimmune encephalomyelitis. *J. Neurosci. Res.*, **67**, 461–470.
64. Katsuno, M., Adachi, H., Doyu, M., Minamiyama, M., Sang, C., Kobayashi, Y., Inukai, A. and Sobue, G. (2003) Leuprorelin rescues polyglutamine-dependent phenotypes in a transgenic mouse model of spinal and bulbar muscular atrophy. *Nat. Med.*, **9**, 768–773.
65. Hamazaki, J., Iemura, S., Natsume, T., Yashiroda, H., Tanaka, K. and Murata, S. (2006) A novel proteasome interacting protein recruits the deubiquitinating enzyme UCH37 to 26S proteasomes. *EMBO J.*, **25**, 4524–4536.
66. Murata, S., Minami, Y., Minami, M., Chiba, T. and Tanaka, K. (2001) CHIP is a chaperone-dependent E3 ligase that ubiquitylates unfolded protein. *EMBO Rep.*, **2**, 1133–1138.
67. Minamiyama, M., Katsuno, M., Adachi, H., Waza, M., Sang, C., Kobayashi, Y., Tanaka, F., Doyu, M., Inukai, A. and Sobue, G. (2004) Sodium butyrate ameliorates phenotypic expression in a transgenic mouse model of spinal and bulbar muscular atrophy. *Hum. Mol. Genet.*, **13**, 1183–1192.
68. Adachi, H., Kume, A., Li, M., Nakagomi, Y., Niwa, H., Do, J., Sang, C., Kobayashi, Y., Doyu, M. and Sobue, G. (2001) Transgenic mice with an expanded CAG repeat controlled by the human AR promoter show polyglutamine nuclear inclusions and neuronal dysfunction without neuronal cell death. *Hum. Mol. Genet.*, **10**, 1039–1048.
69. Hirano, Y., Hayashi, H., Iemura, S., Hendil, K.B., Niwa, S., Kishimoto, T., Kasahara, M., Natsume, T., Tanaka, K. and Murata, S. (2006) Cooperation of multiple chaperones required for the assembly of mammalian 20S proteasomes. *Mol. Cell*, **24**, 977–984.
70. Hamazaki, J., Sasaki, K., Kawahara, H., Hisanaga, S., Tanaka, K. and Murata, S. (2007) Rpn10-mediated degradation of ubiquitinated proteins is essential for mouse development. *Mol. Cell. Biol.*, **27**, 6629–6638.
71. Menendez-Benito, V., Heessen, S. and Dantuma, N.P. (2005) Monitoring of ubiquitin-dependent proteolysis with green fluorescent protein substrates. *Methods Enzymol.*, **399**, 490–511.

ABSTRACT: Spinal and bulbar muscular atrophy (SBMA) is an adult-onset motor neuron disease caused by a CAG repeat expansion in the androgen receptor gene. Because the progression of SBMA is slow, it is plausible to identify biomarkers that monitor disease course for therapeutic development. To verify whether the 6-min walk test (6MWT) is a biomarker of SBMA, we performed the 6MWT in 35 genetically confirmed patients and in 29 age-matched healthy controls. The walk distance covered within 6 min (6MWD) was significantly less in SBMA than it was in controls (323.3 ± 143.9 m and 637.6 ± 94.2 m, respectively; $P < 0.001$). In test–retest analysis, the intraclass correlation coefficient for the 6MWD was high in SBMA patients ($r = 0.982$). In a 1-year follow-up the 6MWD significantly decreased at a rate of 11.3% per year. Our observations suggest that the 6MWT is a biomarker that can be used to monitor progression of motor impairment in SBMA.

Muscle Nerve **38:** 964–971, 2008

WALKING CAPACITY EVALUATED BY THE 6-MINUTE WALK TEST IN SPINAL AND BULBAR MUSCULAR ATROPHY

YU TAKEUCHI, MD,[1] MASAHISA KATSUNO, MD, PhD,[1,2] HARUHIKO BANNO, MD, PhD,[1] KEISUKE SUZUKI, MD, PhD,[1] MOTOSHI KAWASHIMA, MD,[1] NAOKI ATSUTA, MD, PhD,[1] MIZUKI ITO, MD, PhD,[1] HIROHISA WATANABE, MD, PhD,[1] FUMIAKI TANAKA, MD, PhD,[1] and GEN SOBUE, MD, PhD[1]

[1] Department of Neurology, Nagoya University Graduate School of Medicine, 65 Tsurumai-cho, Showa-ku, Nagoya 466-8550, Japan
[2] Institute for Advanced Research, Nagoya University, Nagoya, Japan

Accepted 12 May 2008

Spinal and bulbar muscular atrophy (SBMA) is a hereditary lower motor neuron disease that affects adult males exclusively. It has a prevalence of 1–2 per 100,000 of the total population.[13,20,28] The cause of SBMA is an aberrant elongation of a CAG repeat in the androgen receptor (AR) gene. CAG repeats range from 9 to 36 in normal subjects, but 38 to 62 repeats are found in SBMA patients.[3,22,31,32] CAG repeat expansion has also been detected in Huntington's disease and several forms of spinocerebellar ataxia.[14] The main symptoms of SBMA are weakness and atrophy of the bulbar, facial, and limb muscles. The onset of weakness is usually between 30 and 60 years, followed by slow progression of neuromuscular symptoms.[5] The onset of symptoms and clinical features of SBMA are dependent on the CAG repeat size, as has been observed in other polyglutamine diseases.[10,31]

Although there is no effective treatment for SBMA, several therapeutic candidates have recently emerged from studies in animal models, and clinical trials have been proposed.[18,19,24,33,36] It is, however, difficult to assess the effects of intervention on true disease endpoints such as the occurrence of pneumonia or the length of time a patient lives free from the use of a wheelchair, because the progression of symptoms is notably slow in SBMA.[5] Therefore, appropriate surrogate endpoints are needed to facilitate the clinical application of animal study results. In this regard, it is important to identify biomarkers of SBMA that reflect the pathogenic processes and can be used as surrogate endpoints. Although nuclear accumulation of mutant AR protein in the scrotal skin has been shown to be a candidate for a histopathological biomarker,[1,6] clinical parameters to evaluate motor function have not been established for SBMA.

The 6 min walk test (6MWT) is one of the most popular clinical tests used for assessment of functional capacity. This test evaluates the global and integrated responses of all the systems involved in walking, including the pulmonary and cardiovascular systems, neuromuscular units, muscle metabo-

Abbreviations: 6MWD, 6-min walk distance; 6MWT, 6-min walk test; ALS, amyotrophic lateral sclerosis; ALSFRS-R, ALS functional rating scale-revised; AR, androgen receptor; PCR, polymerase chain reaction; SBMA, spinal and bulbar muscular atrophy

Key words: spinal and bulbar muscular atrophy; 6-minute walk test; biomarker; exercise test; 6-minute walk duration

Correspondence to: G. Sobue; e-mail: sobueg@med.nagoya-u.ac.jp or M. Katsuno; e-mail: ka2no@med.nagoya-u.ac.jp

Published online 21 July 2008 in Wiley InterScience (www.interscience.wiley.com). DOI 10.1002/mus.21077

lism, systemic circulation, peripheral circulation, and blood condition. Because the 6MWT accurately reflects patients' activities of daily living, it has been applied widely for evaluation of functional exercise capacity in cardiopulmonary disorders.[29] It has also been employed to assess functional exercise capacity in neuromuscular diseases such as stroke, Parkinson's disease, cerebral palsy, chronic poliomyelitis, multiple sclerosis, myotonic dystrophy, fibromyalgia, and spinal cord injury.[2,7,8,11,12,16,21,23,25,27] In diseases that affect multiple regions of the nervous system, the 6 min walk distance (6MWD) correlates well with other measurements that evaluate systemic motor function such as muscle strength, clinical scores, and health status questionnaires.[16,23,25]

The aim of this study was to evaluate functional exercise capacity in patients with SBMA using the 6MWT. We also investigated the natural history of the 6MWD in order to determine whether it is an appropriate biomarker that can be used as a surrogate endpoint in forthcoming clinical trials.

MATERIALS AND METHODS

Participants. A total of 35 patients with a diagnosis of SBMA confirmed by genetic analysis were included. Patients were included if they were capable of walking independently along a flat corridor with or without the use of a cane or similar equipment. Exclusion criteria included unstable angina or myocardial infarction during the previous month, tachycardia (>120/min), and uncontrolled hypertension (>180/100 mmHg). We also evaluated 29 age-matched control subjects in this study. The first test was performed between May 2006 and June 2007; reevaluation of 24 of the 35 SBMA patients was conducted ≈1 year after the initial test. The remaining cases were excluded from the follow-up evaluation, because they participated in another interventional study after their first 6MWT evaluation. The age-matched controls did not undergo serial testing.

In addition to the 6MWT, we also evaluated general motor function using clinical scales for amyotrophic lateral sclerosis (ALS), such as the Limb Norris Score, the Norris Bulbar Score, the ALS functional rating scale-revised (ALSFRS-R), and grip power. We defined the onset of disease as the time when muscle weakness began, but not when tremor of the fingers appeared. All studies conformed to the ethics guidelines for human genome/gene analysis research and the ethics guidelines for epidemiological studies endorsed by the Japanese government. The Institutional Review Board of Nagoya University Graduate School of Medicine approved the study, and all SBMA patients and normal subjects gave their informed consent for the investigation.

Six-min Walk Test. The 6MWT was performed according to the guidelines provided by the American Thoracic Society.[4] Briefly, examiners instructed participants to walk at their own pace as far as possible in 6 min. The patients were allowed to rest when needed. No encouragement was made throughout the test. The total distance walked during 6 min (6-min walk distance: 6MWD) was recorded. Patients with severe weakness were permitted to use a cane or equivalent assistive device if needed. The 6MWT was performed along a long, flat, straight, enclosed corridor with turnaround points at an interval of 30 m. Although the time of day was not the same, all tests were performed indoors with the same lighting and temperature. All patients were instructed to wear sneakers or equivalent shoes. The results were based on a single 6MWT. We did not perform repeated tests or practice sessions, because patients with SBMA have severe fatigability, which might produce unstable data and cause safety problems.[26,30,35] In addition to the 6MWD, we also recorded the Borg scale before and after the 6MWT.

To assess reliability the 6MWT was repeated within 60 days after the first test in 15 patients without informing them of the results of the previous test. Likewise, patients were not allowed to know the distance covered in the first test when they took the 1-year follow-up study.

Genetic Analysis. Genomic DNA was extracted from peripheral blood of SBMA patients using conventional techniques.[32] Polymerase chain reaction (PCR) amplification of the CAG repeat in the AR gene was performed using a fluorescein-labeled forward primer (5′-TCCAGAATCTGTTCCAGAGCGTGC-3′) and a nonlabeled reverse primer (5′-TGGCCTCGCTCAGGATGTCTTTAAG-3′). Detailed PCR conditions and measurement of CAG-repeat size were described previously.[10,32]

Data Analysis. All data are presented as means ± SD. Changes in the 6MWD were compared using a paired *t*-test. Correlations among the parameters were analyzed using Pearson's correlation coefficient. *P*-values less than 0.05 and correlation coefficients (r) greater than 0.4 were considered to indicate significance. Calculations were performed using the statistical software package SPSS 14.0J (SPSS Japan, Tokyo, Japan).

RESULTS

Clinical and Genetic Backgrounds of SBMA Patients. The clinical characteristics of the study population are presented in Table 1A. There were a total of 35 subjects in the study. All participants were male and of Japanese nationality. The duration from onset was assessed at the first notice of motor impairment[5] and this ranged from 1 to 32 years. There was no significant difference between the median CAG repeat length in the present study and those reported previously in SBMA patients.[3,22,32] All patients were ambulatory with or without aid, and none were bedridden or wheelchair-bound. Other complications that required medication were found in 33 (94.3%) out of 35 patients: diabetes mellitus in 12 (34.3%), hyperlipidemia in 23 (65.7%), hypertension in 20 (57.1%), and depression in 3 (8.6%). Ischemic heart disease or pulmonary disorders were not documented in any patients included in this study.

Reliability of the 6MWT in SBMA Patients. To estimate test–retest reliability we performed the 6MWT on 15 randomly chosen SBMA patients on two different occasions at an interval of 29.4 ± 10.9 days. There was no statistical difference between the clinical scores of the patients who underwent test–retest analysis and those of the remaining subjects (Table 1B). In each patient the two tests were conducted by different examiners. As shown in Figure 1, when the two sets of the 6MWT were compared with one another the intraclass correlation coefficient was 0.982 ($P < 0.001$), indicating an excellent test–retest reliability for SBMA patients.

6MWD and Relevant Clinical Parameters in SBMA. To verify that the 6MWT detects motor impairment in SBMA patients we compared the data from a total of 35 cases and 29 age-matched control subjects (Table 2). There was a significant difference ($P < 0.001$) in

Table 1. Clinical and genetic features of SBMA patients.

A Clinical and genetic features	Mean ± SD (range)	*n*
Age at examination (years)	55.8 ± 11.2 (33–74)	35
CAG repeat length in AR gene (number)	48.3 ± 3.5 (42–57)	29*
Duration from onset (years)	9.7 ± 7.1 (1–32)	35
Limb Norris Score (normal score = 63)	52.5 ± 7.3 (34–62)	35
Norris Bulbar Score (normal score = 39)	33.3 ± 4.2 (20–39)	35
ALSFRS-R (normal score = 48)	41.2 ± 3.7 (33–47)	35
Grip power (kg)†	18.7 ± 5.3 (8.3–33.9)	33

B	Followed-up group		Non followed-up group		
Clinical and genetic features	Mean ± SD (range)	*n*	Mean ± SD (range)	*n*	*P*
Age at examination (years)	55.3 ± 10.9 (33–70)	24	56.7 ± 12.3 (34–74)	11	NS
CAG repeat length in AR gene (number)	48.6 ± 3.6 (42–57)	19*	47.7 ± 3.4 (42–52)	10*	NS
Duration from onset (years)	10.3 ± 7.7 (1–32)	24	9.4 ± 5.9 (2–21)	11	NS
Limb Norris Score (normal score = 63)	52.3 ± 7.3 (34–62)	24	52.9 ± 7.7 (39–62)	11	NS
Norris Bulbar Score (normal score = 39)	33.3 ± 4.3 (20–39)	24	33.5 ± 4.1 (25–38)	11	NS
ALSFRS-R (normal score = 48)	41.0 ± 3.5 (35–46)	24	41.5 ± 4.2 (33–47)	11	NS
Grip power (kg) †	19.6 ± 4.3 (12.0–27.2)	22	17.0 ± 6.7 (8.3–33.9)	11	NS

C	Retested group		Non retested group		
Clinical and genetic features	Mean ± SD (range)	*n*	Mean ± SD (range)	*n*	*P*
Age at examination (years)	57.0 ± 11.7 (34–74)	15	54.9 ± 11.0 (33–68)	20	NS
CAG repeat length in AR gene (number)	48.4 ± 3.9 (42–57)	14*	48.3 ± 3.2 (42–53)	15*	NS
Duration from onset (years)	9.3 ± 5.6 (2–21)	15	10.5 ± 8.2 (1–32)	20	NS
Limb Norris Score (normal score = 63)	52.7 ± 7.4 (39–62)	15	52.3 ± 7.5 (34–62)	20	NS
Norris Bulbar Score (normal score = 39)	32.7 ± 5.1 (20–38)	15	33.8 ± 3.4 (26–39)	20	NS
ALSFRS-R (normal score = 48)	41.4 ± 4.1 (33–47)	15	41.0 ± 3.4 (35–46)	20	NS
Grip power (kg) †	18.4 ± 6.3 (8.3–33.9)	15	19.0 ± 4.4 (12.0–27.2)	18	NS

Data are shown as mean ± SD.

**The abnormal elongation of the CAG repeat was confirmed by gene analysis using agarose gel electrophoresis without determining the repeat number in the remaining 6 patients.*

† The average of both hands. The normal control data of male Japanese at 50–54 years: 43.7 ± 6.4 kg. (The report of physical strength and athletic capability surveillance in 2005.)

AR, androgen receptor; ALSFRS-R, ALS functional rating scale-revised; NS, not significant.

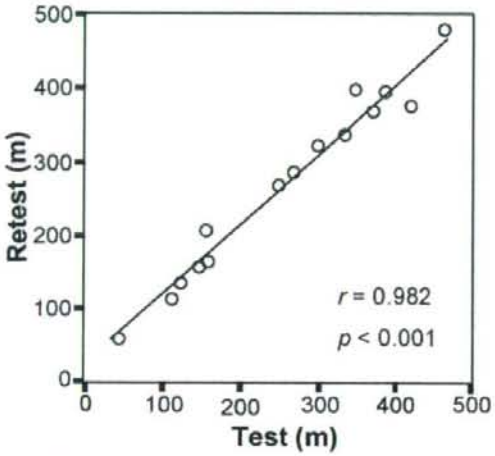

FIGURE 1. Test–retest analysis of the distance walked within 6 min (6MWD). Two sets of 6-min walk tests were carried out within 60 days in 15 SBMA patients who did not know the result of their previous test.

the 6MWD between SBMA patients and the controls. There was no significant difference in the posttest Borg scale, a semiquantitative measure of perceived exercise-related fatigue, between SBMA patients and controls.

We also evaluated motor function of SBMA patients using functional scales and grip power. Because there are no specific motor scores for SBMA we adopted the functional scales used for ALS. The values of the 6MWD correlated well with those of the Limb Norris Score, the Norris Bulbar Score, and the ALSFRS-R (Fig. 2A–C). The value of the 6MWD was inversely correlated with disease duration, although there was no correlation between the 6MWD and grip power (Fig. 2D,E).

Natural History of the 6MWD in SBMA. To delineate the progression rate of walking disturbance the 6MWT was reperformed in a group of 24 SBMA patients at 54.3 ± 6.8 weeks after the initial evaluation. Although follow-up data for the remaining cases was not available because of participation in another interventional study, there was no statistical difference between the backgrounds of the followed subjects and the remaining cases (Table 1C). The 6MWD was significantly decreased in comparison with the distance in the first test ($P = 0.001$), although no motor functional scales showed significant deterioration during the same time period (Table 3). It should be noted that the rate of decline was 11.3 ± 17.6%, which was relatively constant regardless of the walking capacity at the initial evaluation (Fig. 3A). When the patients were stratified by their baseline severity, the change in 6MWD during the follow-up period was larger in the less affected subgroup (Fig. 3B,C).

Based on the natural history of the 6MWD in SBMA, we calculated the sample size for a clinical trial targeting 6MWD, the Limb Norris Score, the Norris Bulbar Score, and ALSFRS-R (Table 4). The sample sizes for a clinical trial using the 6MWT are smaller than those using motor scales, suggesting that it is a more feasible outcome measure than the other clinical scores.

Safety of the 6MWT in SBMA Patients. Throughout the tests, no adverse events such as angina and dyspnea were reported. Although 10 cases walked using a cane and 1 patient walked leaning against a wall, no patients fell or tripped during the tests.

DISCUSSION

This study demonstrates that the 6MWT is a practical, reliable, and safe procedure to measure the walking capacity of SBMA patients. Gait disturbance is the initial symptom in the majority of SBMA patients, and it precedes other health problems such as respiratory failure and dysphagia by ≈10–20 years.[5] Therefore, walking capacity is one of the strongest determining factors of activities of daily living during disease progression in SBMA, implying that the 6MWT appears to be a valuable target for future therapeutic interventions. Although the duration of illness of the patients we tested ranged from 1 to 32 years, our observations suggest that the 6MWT is applicable for patients with various disease durations as long as they are capable of walking.

As a quantitative measure of walking capacity the 6MWT was originally developed for cardiorespiratory and cardiovascular populations. Since then, this test has been applied to various medical conditions including neuromuscular disorders. For example, the 6MWD is strongly correlated with functional

Table 2. Six-min walk distance (6MWD) in SBMA and healthy controls.

	SBMA ($n = 35$)	Healthy controls ($n = 29$)	P
6MWD (m)	323.3 ± 143.9	637.6 ± 94.2	< 0.001
Age at examination (years)	55.8 ± 11.2	52.8 ± 10.7	NS
Borg scale	3.9 ± 2.4	3.2 ± 2.1	NS

Data are shown as mean ± SD.

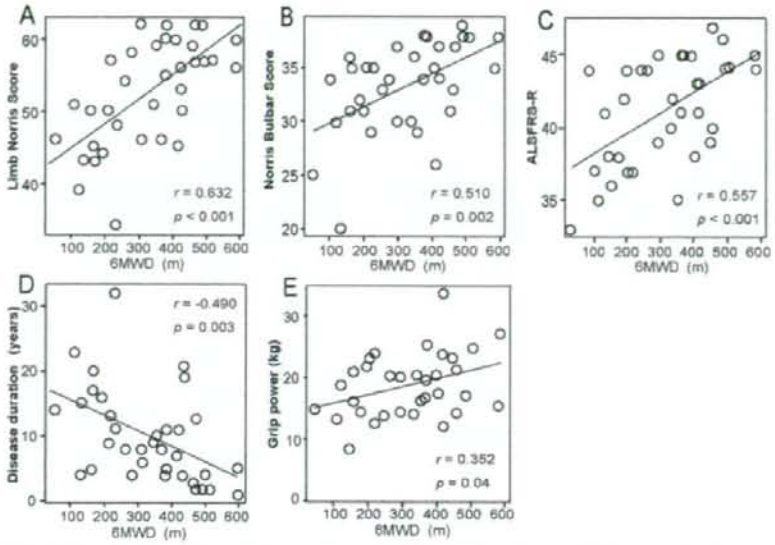

FIGURE 2. Correlation between the 6MWD and other measurements of motor function. **A–C:** The correlation between the 6MWD and general motor function. There was a significant correlation between the 6MWD and motor functional scales such as the Limb Norris Score **(A)**, the Norris Bulbar Score **(B)**, and the ALS functional rating scale-revised (ALSFRS-R, **C**). **D:** The value of the 6MWD was inversely correlated with disease duration. **E:** There was no correlation between the 6MWD and grip power. The value of grip power is shown as the average of left and right hands. 6MWD, six-min walk distance.

scores for balance, strength, and spasticity in post-stroke patients.[12] In patients with multiple sclerosis, the 6MWD is shortened when compared to age-matched healthy controls, reflecting physical function disability.[27] Moreover, the 6MWT has been used as an outcome measurement in various clinical trials for patients with mucopolysaccharidosis, postpolio syndrome, and stroke.[9,15,17,34] Partially due to the small number of patients, there are no established clinical parameters to quantify motor function in SBMA. The total distance covered in 6 min correlated well with motor functional scores in SBMA patients in the present study. Because SBMA is a single gene disorder, various tissues are affected to a similar extent in this disease.[6] This appears to be the reason why 6MWD correlates excellently with clinical scores that reflect disability of other parts of the nervous system affected in SBMA. In addition to muscle weakness, SBMA patients often perceive fatigue during continuous exercise, suggesting that objective measurement to detect the degree of functional endurance is feasible for this disease. Our findings indicate that the 6MWT is a practical examination for measuring functional exercise capacity of patients with SBMA and those with other neurodegenerative diseases.

Table 3. Chronological change in motor function in SBMA.

	n	Initial test	Follow-up	*P*
6MWD (m)	24	351.0 ± 142.8	308.5 ± 132.0	0.001
ALSFRS-R	24	41.0 ± 3.5	39.8 ± 4.0	NS
Limb Norris Score	24	52.3 ± 7.3	50.9 ± 8.2	NS
Norris Bulbar Score	24	33.3 ± 4.3	32.9 ± 4.4	NS

Data are shown as mean ± SD. ALSFRS-R, ALS functional rating scale-revised.

Repeated measurement procedures might result in misleading results, because of practice effect. Therefore, it is important to investigate the reliability of this test in order to determine its feasibility for clinical measurement. Although the 6MWD has been shown to increase only slightly in a second performance a day later, the effect of practice wears off after a week.[4,21] The present study also demonstrated that the reliability of the 6MWT is excellent for SBMA patients, if they are tested within an interval of ≈1 month.

Given the rapid advance of therapeutic developments in animal studies, it is a high priority to search for biomarkers to determine disease severity and

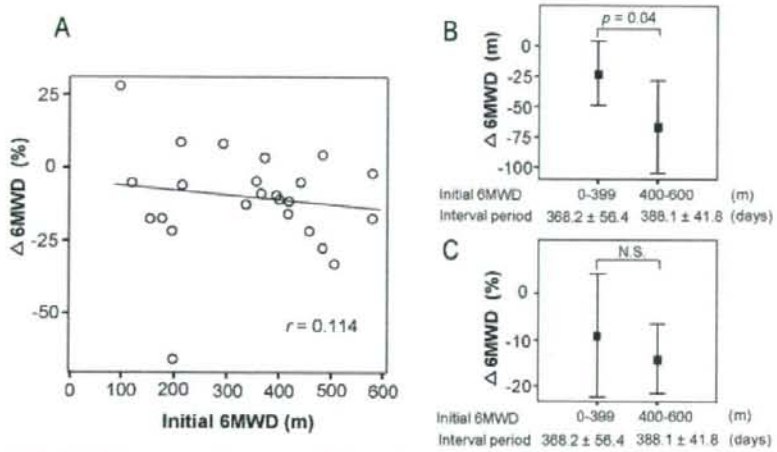

FIGURE 3. The relationship between the change in the 6MWD and the distance in the initial test. **A:** The decline in the 6MWD did not correlate with the result of the initial evaluation. **B,C:** The decline in the 6MWD for each of the severity groups (**B,** actual change; **C,** % change). There was no statistical difference in the follow-up period between both groups.

progression in SBMA. A biomarker is an objectively measurable parameter that indicates the pathogenic process and potentially serves as a surrogate endpoint in a treatment trial. Candidates for biomarkers in neurodegenerative diseases include: motor functional scales; serological parameters; electrophysiological data; histopathological findings; and neuroimaging parameters. It is feasible to analyze combinations of biomarkers to monitor disease progression. There are an increasing number of biomarkers for Alzheimer's disease, but there is a paucity of biomarkers identified in other neurodegenerative diseases. In fact, identification of biomarkers has been hampered by small numbers of patients, slow disease progression, and lack of objective clinical measurements for SBMA. In the present study the 6MWD was significantly decreased in patients with SBMA compared with age-matched healthy subjects, and it correlated well with other scores that measure general motor function. This suggests that the test is capable of detecting motor impairment in SBMA patients. Furthermore, our longitudinal analysis showed that the 6MWD decreases by ≈10% per year in SBMA patients despite no detectable deterioration in the other motor functional parameters we examined. According to our sample size calculation, the number required for a clinical trial appears to be reduced to one-fifth by changing the endpoint from motor scores to 6MWD. For example, when the therapeutic effect is estimated to be 50%, a trial targeting ALSFRS-R needs 500 patients, but the size is diminished to 100 by adopting 6MWD as the endpoint (Table 4). Although it is a limitation of this study that the follow-up data for 11 out of 35 cases was not obtained, there was no statistical difference between the backgrounds of the followed subjects and the remaining cases. This suggests that the 24 patients who underwent the follow-up study represent the whole group. Because the interval between the onset of weakness and the need for a wheelchair has been reported to be ≈15 years, the observed rate of decrease in the 6MWD is likely reasonable.[5] Therefore, our findings also suggest that the 6MWT is an indicator of disease progression, which can be used as an outcome measurement in future clinical trials for SBMA. Our observation that the annual change in 6MWD is influenced by the disease severity might suggest the need for stratification in the design of clinical trials. Given that scrotal skin biopsy analysis is

Table 4. Sample size calculation.

	Estimated therapeutic effect (%)	
Outcome measure	50	70
6MWD	102	52
ALSFRS-R	508	259
Limb Norris Score	462	236
Norris Bulbar Score	2,650	1,352

Data are shown as the number of patients per group (P = 0.05, power = 0.8).
ALSFRS-R, ALS functional rating scale-revised.